Mechanical Properties and Microstructural Characterization of Aged Nickel-based Alloy 625 Weld Metal

CLEITON CARVALHO SILVA, VICTOR HUGO C. DE ALBUQUERQUE, EMERSON MENDONÇA MINÁ, ELINEUDO P. MOURA, and JOÃO MANUEL R.S. TAVARES

The aim of this work was to evaluate the different phases formed during solidification and after thermal aging of the as-welded 625 nickel-based alloy, as well as the influence of microstructural changes on the mechanical properties. The experiments addressed aging temperatures of 650 and 950 °C for 10, 100, and 200 hours. The samples were analyzed by electron microscopy, microanalysis, and X-ray diffraction in order to identify the secondary phases. Mechanical tests such as hardness, microhardness, and Charpy-V impact test were performed. Nondestructive ultrasonic inspection was also conducted to correlate the acquired signals with mechanical and microstructural properties. The results show that the alloy under study experienced microstructural changes when aged at 650 °C. The aging was responsible by the dissolution of the Laves phase formed during the solidification and the appearance of γ'' phase within interdendritic region and fine carbides along the solidification grain boundaries. However, when it was aged at 950 °C, the Laves phase was continuously dissolved and the excess Nb caused the precipitation of the δ-phase (Ni_3Nb), which was intensified at 10 hours of aging, with subsequent dissolution for longer periods such as 200 hours. Even when subjected to significant microstructural changes, the mechanical properties, especially toughness, were not sensitive to the dissolution and/or precipitation of the secondary phases.

https://doi.org/10.1007/s11661-018-4526-2

I. INTRODUCTION

ONE of the most interesting characteristics of the nickel-based superalloys is its high corrosion resistance to an aqueous chloride medium.[1] Furthermore, these alloys exhibit extraordinary resistance to a wide range of organic and mineral acids due to their excellent corrosion resistance properties, mainly, at high temperatures, and, therefore, are commonly found in the marine, aerospace, chemical, and oil and gas industries.[2–5]

The alloy Inconel® 625 stands out as one of the leading commercial Ni-Cr-Mo-Nb alloy grades.[2] The development of this alloy in 1964 was designed to meet the market of alloys for high-temperature service. However, with the discovery of its exceptional corrosion resistance, it also came to assume a prominent position in other applications, where corrosion resistance is essential.[1]

In addition, the 625 nickel-based superalloy exhibits an outstanding combination of mechanical properties and resistance to pitting, crevice and intergranular corrosion due to the solid-solution strengthening effect of chromium, molybdenum and niobium in its nickel matrix, making precipitation-hardening treatments unnecessary.[1] However, elements such as Cr, Ti, Nb, and Mo are also strong precipitate formers. According to many studies, the presence of these elements influences the formation of the metastable γ'' phase (Ni_3Nb), primary MC carbides where M denotes Nb and Ti. There are other types of carbides such as M_6C, where M denotes Si, Ni, and Cr, and also $M_{23}C_6$ where M denotes mainly Cr and/or Mo.[6–9]

Nevertheless, the high cost of nickel-based superalloys makes them unviable for massive applications in some situations. In order to overcome this obstacle and make the use of Ni-based alloys attractive to equipment

CLEITON CARVALHO SILVA, EMERSON MENDONÇA MINÁ, and ELINEUDO P. MOURA are with the Departamento de Engenharia Metalúrgica e de Materiais, Universidade Federal do Ceará, Fortaleza, Ceará, Brazil. Contact e-mail: cleiton@metalmat.ufc.br VICTOR HUGO C. DE ALBUQUERQUE is with the Programa de Pós-Graduação em Informática Aplicada, Universidade de Fortaleza, Fortaleza, Ceará, Brazil. JOÃO MANUEL R.S. TAVARES is with the Departamento de Engenharia Mecânica, Faculdade de Engenharia, Instituto de Ciência e Inovação em Engenharia Mecânica e Engenharia Industrial, Universidade do Porto, Porto, Portugal.

Manuscript submitted June 25, 2017.
Article published online March 7, 2018

manufacturers, providing high service performance using this particular class of material overlays with Ni-based alloys on C-Mn low alloy and stainless steels have become an option in recent years.[10–12]

During welding with the Inconel 625 alloy as filler metal, there is an intense microsegregation of elements, such as niobium and molybdenum, within the interdendritic regions causing the supersaturation of the liquid metal in its final stage of solidification.[10] This important phenomenon results in the precipitation of Nb-rich Laves phase and MC primary carbides of type NbC.[13,14] The segregation and precipitation of secondary phases like Nb-rich Laves phase, which has a low melting point, can cause an increase in the temperature solidification range, making the alloy susceptible to solidification cracking.[15] However, an adequate selection of the welding conditions can minimize the formation of the Nb-rich Laves phases, thus reducing susceptible to solidification cracking.

Although several studies have reported the presence of Laves phase in alloys containing Nb and Mo, such as 625 and 718, there are few studies that address the effect of the presence of this phase on the mechanical properties, especially impact resistance.[16,17] However, there are several studies on the effect of high-temperature exposure on secondary phase precipitation, and the effect of such precipitations on the mechanical properties has been investigated.[18–21] Nonetheless, on many occasions, these alloys are evaluated from wrought or annealing bars, which present very different properties when compared with the ones of the alloys in their as-welded condition.

As a general rule, the microstructural changes in these alloys, and consequently changes to their mechanical properties, have been extensively investigated using metallographic evaluations supported by microscopic techniques. However, these investigations can be difficult, especially in field applications where access to the affected areas may be restricted.[22] Recently, the potential of nondestructive testing methods, based on ultrasonic signals, to evaluate microstructural characterization and mechanical properties in ferrous alloys have been systematically evaluated. The authors analyzed ultrasonic results of velocity and attenuation and compared them against the ones obtained by destructive testing such as the Charpy impact, X-ray diffraction, and hardness tests.[23–25] The findings showed that ultrasonic testing is a promising technique to follow-up material phase transformations. Regarding the 625 alloy, this nondestructive approach was successfully used to detect the microstructural changes of the alloy based on ultrasonic attenuation and velocity measurements by Albuquerque *et al.*[26]

Besides such approaches, further research work has been developed to obtain faster and more accurate methods for microstructural characterization. Such research has included the automated classification of the acquired ultrasonic signals classification using Optimum Path Forest,[27] Support Vector Machine, Bayesian and Artificial Neural Network based classifiers.[28] Results with over 90 pct accuracy have been achieved in 1.40 ± 0.57 ms with material samples aged at 650 °C and aging times of 0, 10, 100, 200 hours. However, the performance of these techniques is lower for samples aged at temperatures of 950 °C for the same time periods, presenting an accuracy of approximately 73 pct in 0.77 ± 0.02 ms.

Recently, Silva *et al.*[29] evaluated the performance of magnetic permeability as a nondestructive low-cost and alternative tool for the microstructural characterization of a duplex stainless steel. These authors showed that magnetic permeability based on a Hall effect sensor can be used to follow-up the formation of an α' phase from an α phase in a duplex stainless steel.

Several studies in the literature have evaluated the microstructural evolution under aging treatments for wrought, rolled, sintered, or annealed conditions.[30–33] On the other hand, there are few studies evaluating the solidification structures produced by casting, welding or additive manufacturing, under aging treatments.[33–35] Slight differences in terms of the chemical composition, solidification parameters, and original microstructures may affect the precipitation behavior of these alloys. Therefore, the range of the operating conditions exploited, especially with reference to the welding conditions must be extended and investigated. The present work carried out a detailed investigation of a 625 nickel-based alloy weld cladding, deposited using high heat input, in order to explore the effects of the original solidified state in terms of microstructure and microchemistry, on microstructural evolution and mechanical properties under conditions of thermal aging at temperatures of 650 °C and 950 °C with different aging times.

II. EXPERIMENTAL PROCEDURES

Nickel-based 625 alloy coatings deposited on an ASTM A36 steel base were used in the experiments. The chemical compositions of these materials are shown in Table I. A 4.0-mm diameter tungsten electrode doped with thorium was used, and pure argon (99.99 pct) was chosen as the shielding gas.

An electronic multi-process power source connected to the data acquisition system was used during the welding to monitor the current and tension applied. The manipulation of the torch was carried out using an industrial robot system, Figure 1(a). An automatic cold wire feed system for the gas tungsten arc welding (GTAW) was used to supply the filler metal. A positioning unit was used to guide the wire into the arc so that adjustments to the configuration parameters and geometry of the wire feed could be made, Figure 1(b).

The coating was welded onto an ASTM A36 steel base plate, resulting in a coating of 350 × 60 × 14 mm.[3] The other welding parameters were as follows: 285 A of welding current (DCEN), arc voltage of 20 V, travel speed equal to 21 cm/min, welding heat input of 16 kJ/cm, wire feed speed equal to 6.0 m/min, arc length of 10 mm, 15 l/min of gas flow, and arc oscillation describing a double-8 trajectory. Other minor settings included the wire feed direction ahead of the arc weld, wire tip to

Table I. Chemical Composition in Percent Weight of the Weld Metal/Coating and Base Metal

	Ni	C	Cr	Mo	W	Fe	Al	Ti	Nb	Mn	Si	Cu	Co	V	P	S
AWS ERNiCrMo-3 (INCONEL 625 alloy—Weld Metal)	64.43	0.011	22.2	9.13	—	0.19	0.09	0.23	3.53	0.01	0.05	0.01	0.03	—	0.002	0.002

	Ni	C	Cr	Mo	Fe	Al	Mn	Si
ASTM A36 Steel (Base Metal)	0.01	0.15	0.02	0.01	balance	0.02	0.95	0.2

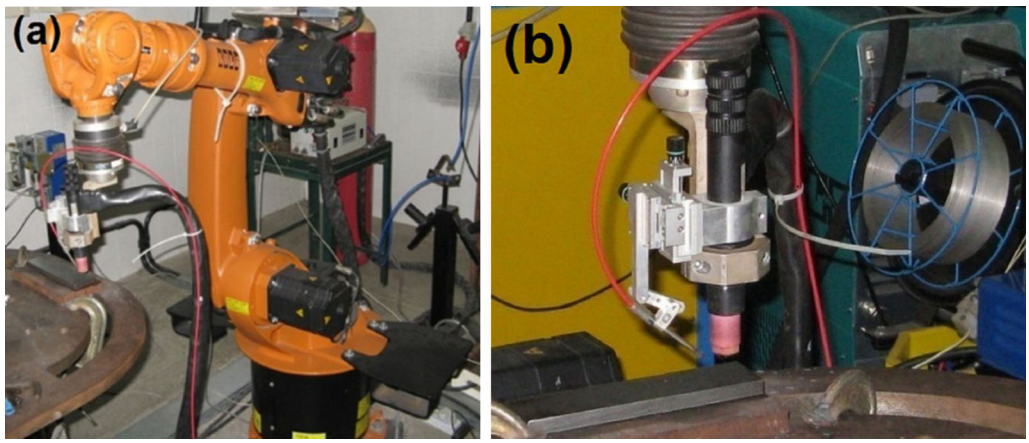

Fig. 1—Experimental setup used in the welding process: (*a*) robotic system, (*b*) GTAW guide wire feed and torch.

pool surface kept at a distance of 3 mm, wire feeding angle maintained constant and equal to 50 deg, and electrode tip angle fixed at 50 deg.

To guarantee a good overlaying due to multiple pass deposited side by side, a distance equal to 2/3 of the initial weld bead width was established as an ideal step. Other arc oscillating parameters adopted were as follows: oscillation amplitude of 8 mm and wave length equal to 1.2 mm. To produce a 10-mm-thick coating on the substrate, seven layers with eight passes were deposited under identical welding conditions.

After the welding, the coating was detached from the substrate by conventional machining, as the material of interest was only the Inconel 625 alloy. Then, the coating was divided into seven plates, three plates were submitted to aging heat treatments at 650 °C for times of 10, 100, and 200 hours, another three plates were submitted to aging heat treatments at 950 °C for times of 10, 100, and 200 hours, and the remaining plate was kept in the as-welded state (0 hour). The aged plates were water cooled with moderate agitation at room temperature.

Afterwards, the seven samples were cut and subjected to metallographic preparation that included grinding using silicon paper with several granulometries, followed by mechanical polishing using diamond paste with 3 and 1 μm. Electrolytic etching using aqueous solution with 10 pct chromic acid under 2.0 V for 15 seconds was used to reveal the nickel-based alloy microstructure. Microstructural analysis of all samples was performed by a scanning electron microscope (SEM) Philips XL30 (Oxford Instruments, England), and a study of the chemical composition of the secondary phases was carried out through energy dispersive spectroscopy of X-rays (EDS).

Another electrochemical etching using perchloric acid (10 pct in volume) in methanol was tested, according to the literature recommendation.[8] Samples subject to this etching were intended for nanosized γ'' phase particles' observations. These analyses were performed using a FEI Quanta 450 Field Emission Gun SEM using secondary electron (SE) operation mode, under magnifications up to 200,000 times.

X-ray diffraction analysis (XRD) was also used to characterize the secondary phases precipitated during solidification and due to solid-state transformation during aging treatment. Since the quantities and dimension of the particles are quite small, an alternative evaluation was carried out according to the ASTM 936 standard, which covers the procedures for the isolation of TCP (topologically close-packed) in nickel-based alloys. The Panalytical XPert Pro MPD X-ray spectrometer was used in the present investigation. For post-processing and peak matching, the X'Pert HighScore software and its database were used. The scan details applied in these analyses were as follows: 2 Theta range from 10 to 120 deg with a step size of approximately 0.02 deg and counting at each step for 4 seconds; Cu Kα radiation was used and the X-ray generator power was set at 40 kV and 40 mA.

To evaluate the influence of TCP precipitation on mechanical performance of weld metals, the Charpy impact test was performed according to ASTM E23 using with 55 × 10 × 10 mm^3 specimens with a 45 deg V-notch, a notch radius of 0.25 mm, and a notch depth of 2 mm. The impact tests for all conditions were performed at room temperature. Five test specimens were evaluated for each condition, and a statistical analysis of variance was performed to evaluate the influence of aging on impact toughness. The microhardness test was performed on the as-welded and aged samples with a Vickers hardness tester Shimadzu (HVMG) using a 200-g load and a dwell time of 15 seconds. Ten indentations were performed randomly along the weld metal cross section, and, again, a statistical analysis of variance was performed to evaluate the influence of aging on hardness.

For the physical property assessment *via* ultrasonic nondestructive testing (also known as ultrasonic NDT), the pulse echo technique was used to obtain the average ultrasonic velocity and attenuation measurements considering twenty signals acquired with 10,000 points, sampling rate of 1 Gs/s, and ultrasonic transducers of 4 and 5 MHz.

For each sample, twenty signals with two adjacent echoes per signal were acquired for the velocity measurements. Next, the time between the first two echoes was measured through an echo overlapping algorithm.[36] With the wave propagation time and the thicknesses of the samples, obtained by using a micrometer at the same signal acquisition points, it was possible to determine the average velocity of wave propagation through the equation:[37]

$$v = \frac{2X}{\tau_0}, \qquad [1]$$

in which X is the thickness of the sample [m] and τ_0 is the time of the wave course [s] until the two adjacent echoes (B_1 and B_2) overlap each other, and its value is determined using[37]

$$\left| \int_{-\infty}^{\infty} B_1(t).B_2(t-\tau)P\mathrm{d}t \right|. \qquad [2]$$

Although the time measurement can be obtained directly from the oscilloscope, as previously mentioned, the echo overlapping method was used as it provides greater sensitivity and greater accuracy.[36]

The ultrasonic attenuation coefficient, α [dB/mm], was calculated using[37]

$$\alpha = \frac{20}{2x}\log\frac{A_0}{A_1}, \qquad [3]$$

where x is the thickness of the sample [mm]; A_0 is the amplitude of the first echo [dB]; and A_1 is the amplitude of the second echo [dB]; more details can be found in Normando *et al.*[36]

III. RESULTS

A. *Microstructural Characterization*

The microstructures of the coatings deposited with Inconel 625 alloy by the GTAW cold wire feed process were analyzed by SEM, and the results revealed a Ni-fcc matrix that solidified in a cellular/dendritic mode. During the solidification process, an intense Mo and Nb microsegregation occurred. Due to this particular phenomenon, extensive amounts of secondary phases were formed at the intercellular or interdendritic regions. An example of the representative microstructure of the as-welded alloy condition (0 hour) is shown in Figure 2(a), which also shows in detail the secondary phase formed in the interdendritic region, confirming the large amount of these secondary phases. Figure 2(b) shows that there are two different types of particles. The first is a bright phase with a shapeless or eutectic morphology, which is due to this phase taking on the shape of the remaining liquid volume during solidification. The second is a faceted or cubic morphology, which is indicated in the figure.

The chemical composition obtained by EDS in some of these phases, indicated an enrichment of Mo and Nb, as well as the presence of Si at higher concentrations (Figure 2(c)). With reference to the other elements, such as Ni, Fe, and Cr, a lower concentration in the secondary phase was found relatively to the nominal composition of the weld metal, Table II. SEM/EDS analysis performed on the cubic precipitate showed higher concentrations of Nb and Ti and lower concentrations of Cr, Ni, and Mo (Figure 2(d)). It is important to point that the MoLα peak overlaps with Nb Lα. In addition, a NKα peak was found. The concentration of the main elements is shown in Table II.

Figures 3, 4, and 5 show the micrographs of the aged samples at 650 °C for 10, 100, and 200 hours, respectively, with the related microstructural modifications perceptible. These micrographs show that the microstructural evolution is mainly due to dissolution of the Nb-rich Laves phase, and the cubic particles of Nb and Ti complex carbides/nitrides remain in the microstructure.

A representative microstructure of the sample aged at 650 °C for 10 hours is shown in Figure 3. There was a very low tendency for the dissolution of Laves phase particles. For the sample aged at 650 °C for 100 hours, an intense dissolution of Laves phase is evident. The volume fraction of the phase reduced greatly compared to the initial conditions (Figure 4). As to the microstructure for the aged condition of 200 hours at a temperature of 650 °C, there was almost a total dissolution of the Laves phase, and only remnants were perceived in the microstructure, as can been verified in Figure 5. In this case, the microstructure consisted almost entirely of the γ-fcc matrix and the particles of cubic NbTi complex carbides/nitrides.

In addition, there was also a noticeable trend in the aged samples with further precipitation after 100 and 200 hours, especially along solidification grain bound-

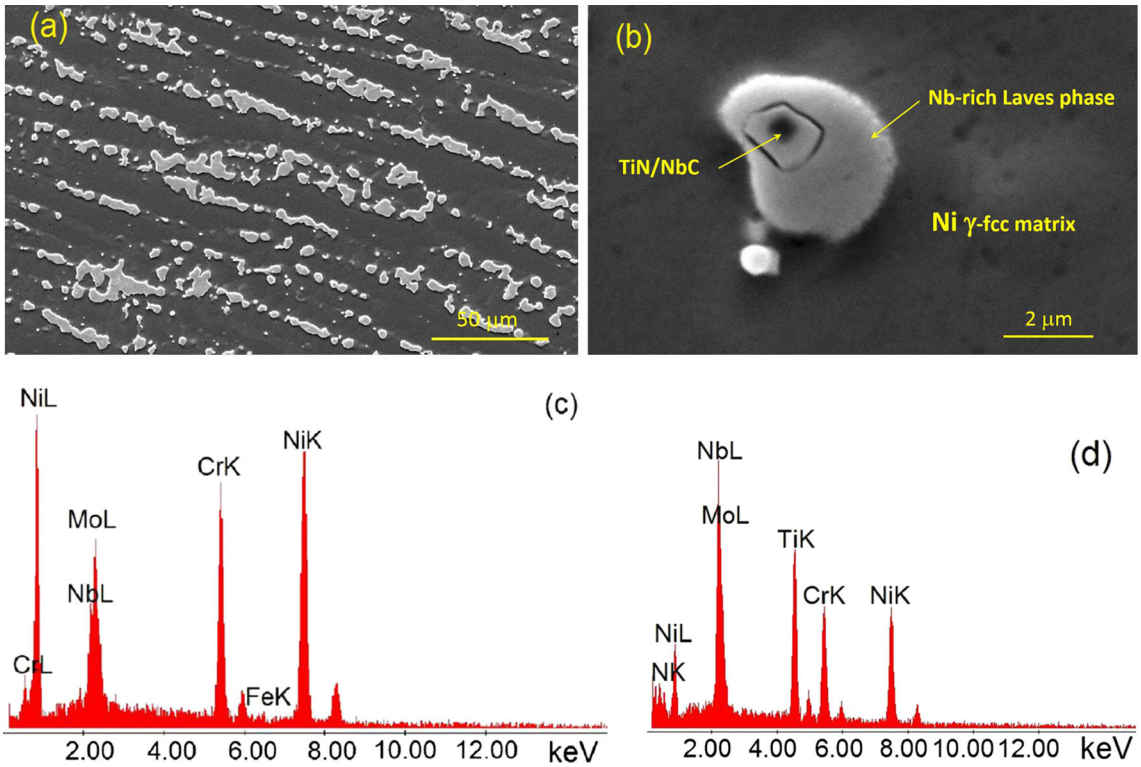

Fig. 2—(*a*) SEM micrographs using secondary electrons showing the Ni-fcc matrix and the secondary phases of the sample as-welded; (*b*) in detail, an agglomerate formed by a cuboidal precipitate of NbC/TiN wrapped by Nb-rich Laves phase; (*c*) EDS spectrum of Laves phase, (*d*) EDS spectrum of NbC/TiN cuboidal precipitate.

Table II. Results of the Chemical Composition Analysis Performed by SEM/EDS on: Laves Phase and Complex NbTi Carbide/Nitride

Laves Phase		NbTi Carbide/Nitride	
Element	Wt Pct	Element	Wt Pct
NbK	18.29	NK	6.37
MoL	21.18	NbL	25.23
CrK	17.27	MoL	8.39
NiK	43.26	TiK	15.60
—	—	CrK	13.88
—	—	NiK	30.52

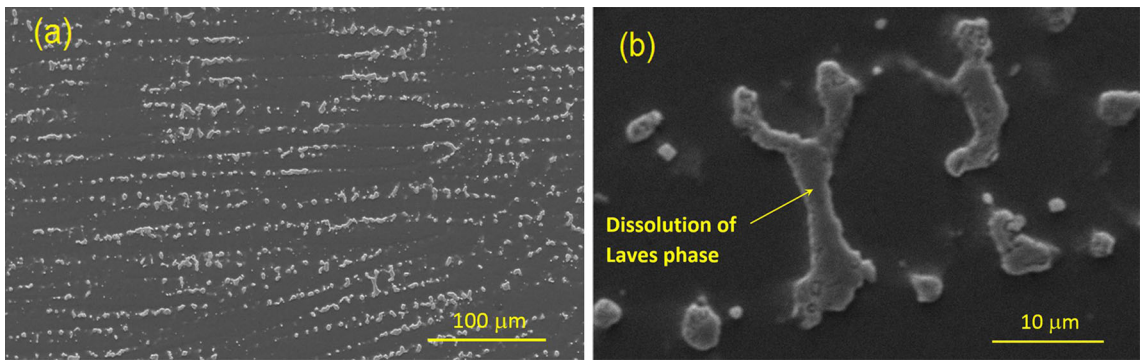

Fig. 3—(*a*) Representative microstructure of the sample aged at 650 °C for 10 h; (*b*) detail of the Eutectic-like Laves phase and some cuboidal precipitates of NbTi carbides/nitrides.

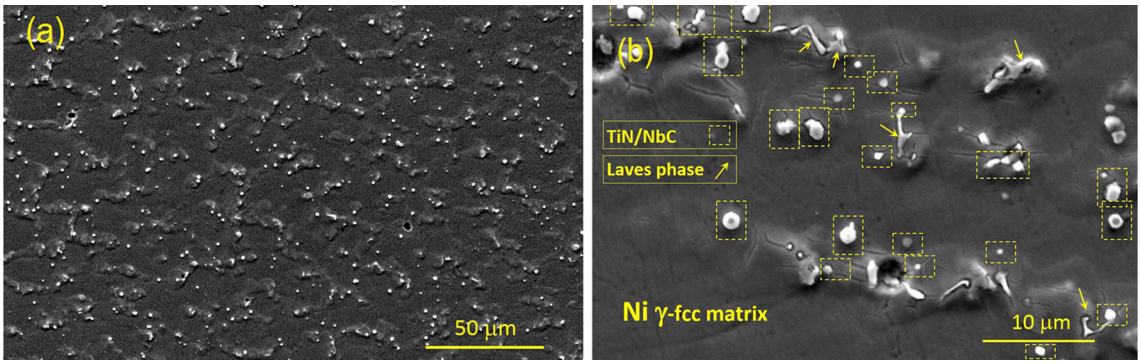

Fig. 4—(*a*) Representative microstructure of the sample aged at 650 °C for 100 h; (*b*) detail decomposition of the Laves phase with significantly reduced dimensions, and where some cuboidal precipitates of carbides/nitrides can also be seen.

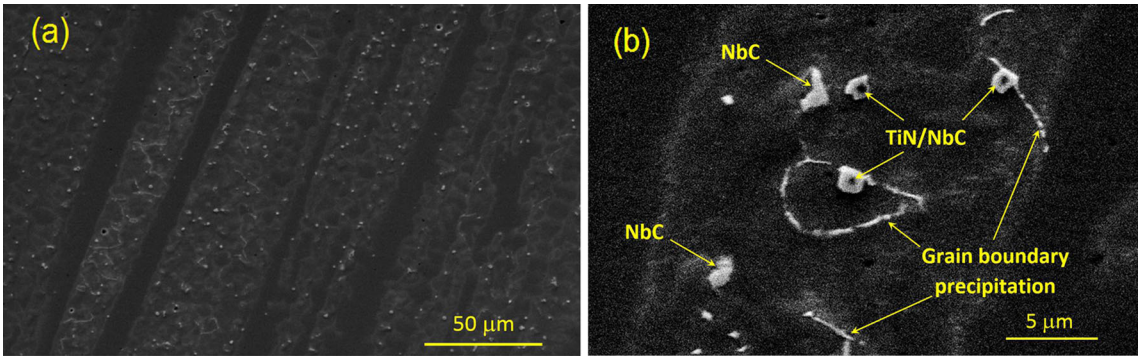

Fig. 5—(*a*) Representative microstructure of the sample aged at 650 °C for 200 h showing practically only NbTi carbides/nitrides; (*b*) detail showing a small particle of Laves phase reminiscent of the incomplete decomposition.

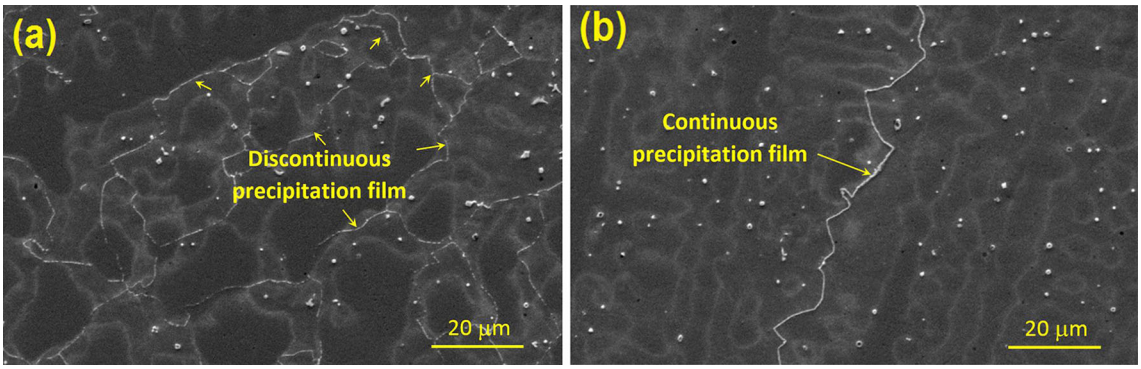

Fig. 6—(*a*) Grain boundary precipitation in an early stage observed in the sample aged at 650 °C for 100 h; (*b*) grain boundary precipitation like a continuous film observed in the sample aged at 650 °C for 200 h.

aries and sub-grain boundaries. Figure 6(a) clearly shows the behavior of the precipitation for the 100 hours aging condition, in which a discontinuous precipitation of very thin precipitates can be seen along the grain boundaries. For the 200 hours aging, a continuous thin film precipitate can be seen along the grain boundaries in Figure 6(b).

Using a low accelerating voltage in a SEM-FEG microscope, EDS analyses of some particles precipitated at the grain boundary were performed (Figure 7(a)). Unfortunately, due to the size of those particles precipitated along the grain boundary, the results of the EDS analysis were not conclusive. However, a slight increase in Cr in these particles and an intense peak of carbon and silicon were found in many cases (Figure 7(b)). This may indicate the formation of carbides such as (Cr_6C) and/or $(CrMo)_{23}C_6$. Also, there was a higher concentration of Nb in the matrix than in the interdendritic region, indicating an enrichment caused by Laves phase dissolution (Figure 7(c)).

According to the Thermo-Calc analysis for the chemical composition of the weld metal evaluated by optical emission spectroscopy (Table III), $M_{23}C_6$ is able

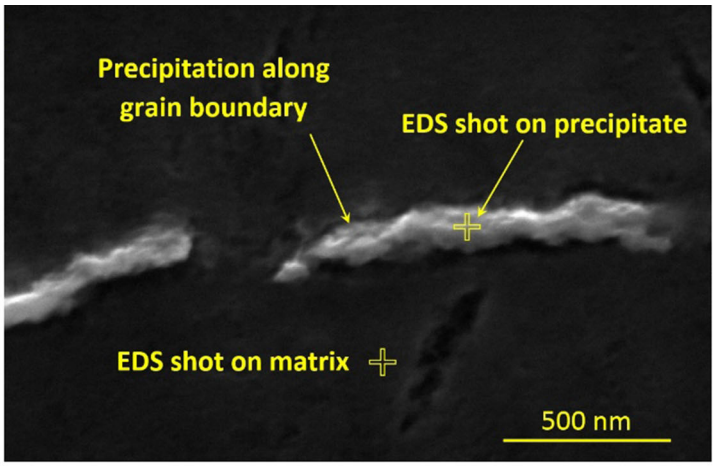

(a)

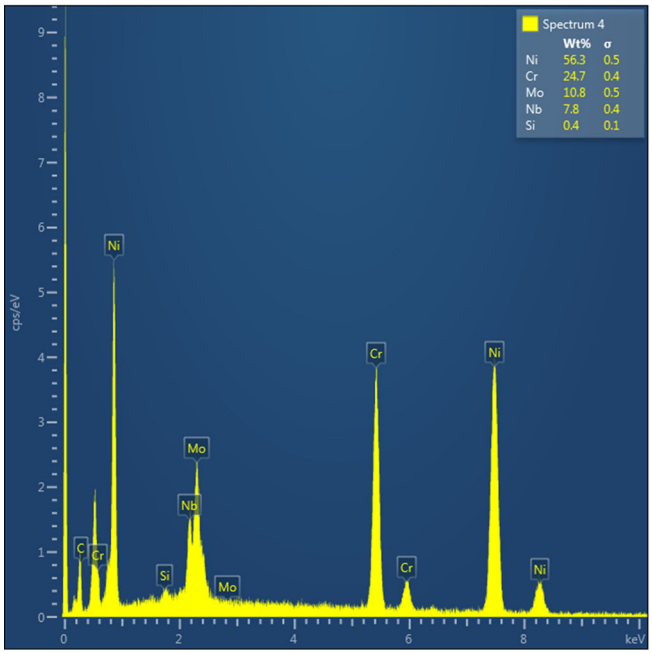

(b)

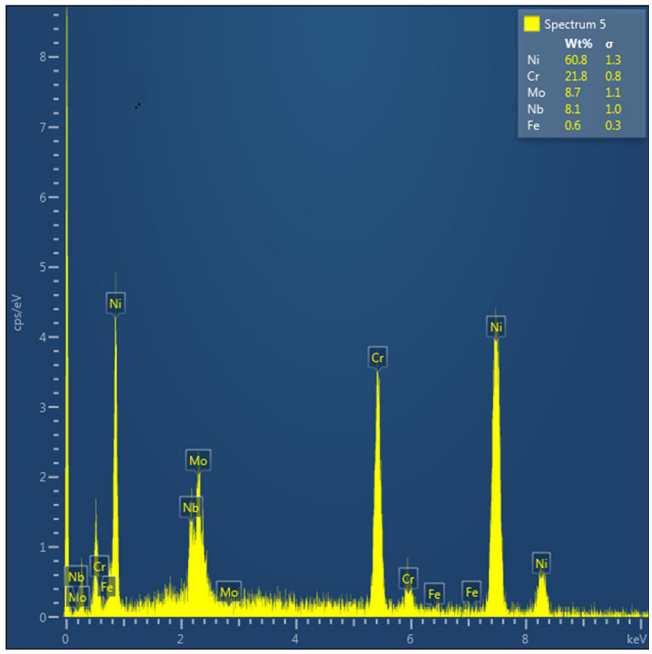

(c)

Fig. 7—(*a*) Microchemical analysis of nanosized precipitates along the grain boundary performed by EDS; (*b*) EDS spectrum of the particle; and (*c*) spectrum of the matrix adjacent to the precipitate.

Table III. Mean Weld Metal Chemical Composition in Weight Percent

C	Cr	Mo	Nb	Fe	Ti	Si	Ni
0.1	21.51	7.455	3.285	2.31	0.665	0.145	balance

to precipitate at all temperatures evaluated in this study (Figure 8). Therefore, $M_{23}C_6$ is considered a strong candidate to precipitate in grain boundaries as it was found at 650 °C after 200 hours.

However, the formation of M_6C carbides cannot be discarded, since these carbides are frequently found in alloys containing chromium, molybdenum, and niobium.[38] In addition, it is reported that M_6C exhibits excellent temperature stability; however, it may undergo a transformation to $M_{23}C_6$ for long exposure time at high temperature (816 °C to 927 °C).[38] In addition, Figure 9 shows the presence of a very thin precipitation along the interdendritic region, together with grain boundary precipitation.

Based on microstructural results found in the literature, it was performed a second electrolytic etching as described in experimental procedure (Section II). This etching resulted in a colored aspect of the microstructure when observed by light microscopy, revealing the solidification dendritic pattern of the weld, as shown

in Figure 10(a). Observing in detail the microstructure, it was found a white region (W), which correspond to the dendritic core (Figure 10(b)). In addition, two other regions were observed, being one in blue (B) and another dyed purple (P).

Microstructural analysis performed using high-resolution scanning electron microscopy revealed the presence of γ'' phase with nanometric size. The γ'' Ni_3Nb phase has the same stoichiometry of the Ni_3Nb δ-phase, but diverges in terms of the crystallographic structure, as it is a body-centered tetragonal (DO22).[20,21,39] In addition, this analysis indicated occurs a heterogeneous nucleation pattern of precipitates along the weld metal, which is directly related to the color pattern observed by LM (Figures 10(a) and (b)). A detailed assessment of these regions confirms the heterogeneous pattern of nucleation, as shown in Figure 10(c). According to these analyses, no evidence of precipitation was observed for the white region (W), which corresponds to dendrite core. The dyed purple region (P) indicated in LM (Figure 10(b)) presented a small content of precipitates; however, the particle size precipitated was apparently greater than particles observed in blue region. Finally, the region in which the greater precipitation of γ'' phase was precisely inside the blue region was observed in LM analysis. Additionally, in this specific region, large cubic NbTi complex carbides/nitrides were found. Figure 10(d) and (e) shows the intense precipitation of γ'' phase observed in high-resolution SEM-FEG analysis. The microstructure observed in this region was similar to results reported in the literature.[8]

On increasing the aging temperature from 650 to 950 °C, several microstructural changes were found. Figure 11 shows representative microstructures of the Inconel 625 alloy aged at 950 °C for 10 hours. In this case, the microstructure indicated the appearance of a new structure with needle morphology. As can be seen in Figure 12, the needles precipitated into the interdendritic region. Another observation is that the Laves phase apparently dissolved to give a needle phase.

A chemical mapping acquired by EDS analysis for the main alloying elements is shown in Figure 13. The results indicated that the region where needles are precipitated is rich in Nb. This suggests that the precipitation occurred preferably in the interdendritic region, since due to microsegregation, this zone is enriched in Nb. This region also has a high volume fraction of Laves phase rich in Nb, which is indicated in Figure 13 by a dotted ellipse, and whose dissolution serves as a continuous supply of Nb to form the needle particles. No alterations were seen in the NbTi complex carbide/nitrides, or in the microstructure (indicated in the chemical maps of Figure 13 by a dotted square).

The 625 alloy weld metal showed a partial dissolution of the δ-phase up to 100 hours aged at 950 °C, as shown in Figure 14(a). In addition, several particles of the cubic complex carbides/nitrides and large blocks of NbC carbides that grew from preexisting carbides/nitrides can be perceived. Also, but with a lower frequency, small particles of Laves phase were found, which were almost completely solutionized during the aging.

Figure 14(b) shows an early stage of nucleation of thin particles mainly precipitated along grain boundaries and sub-grain boundaries. Figures 15(a) and (b) detail the microstructure of the sample aged at 950 °C for 100 hours and depict the apparent dissolution of the Ni_3Nb δ-phase needles and the presence of residual Nb-rich Laves phases in the interdendritic region. Additionally, some small cubic precipitates of the NbTi complex carbide/nitrite can be observed.

Figures 16(a) and (b) show representative micrographs of the treated material held at high temperatures for periods of up to 200 hours. Here, these figures show an almost complete dissolution of the precipitates previously present in the microstructure. No precipitates with needled morphology can be perceived, indicating that for this condition of aging, there was a complete dissolution of the δ-phase. Furthermore, Laves phase particles were not clearly observed, indicating also the complete dissolution of this phase. Therefore, for this condition of treatment, all TCP phases were dissolved and only cubic NbTi carbides/nitrides and large NbC carbides were present in the microstructure. In some regions, where there were no large blocks of primary carbides (NbC), a fine precipitation along the grain boundaries and sub-grain boundaries together with the cubic NbTi carbides/nitrides can be realized, as shown in Figures 16(c) and (d).

In order to increase the volume fraction of the analyzed material, increasing the peak intensities and to improve the identification of the phases formed in the weld metal, X-ray diffraction analyses were performed on powder precipitates produced by the extraction technique in accordance with ASTM A923. XRD results showed the whole X-ray diffractogram recorded for the 10 hours aged sample for the two temperatures: 650 and 950 °C (Figure 17).

All the peaks were identified and indexed according to the standards, depending on the phases formed. For the sample aged at 650 °C for 10 hours (Figure 17(a)), the peaks corresponded to Laves phase, (Nb,Ti)C carbide and γ-fcc matrix, which confirms the microstructural observations made by SEM. Some minor peaks were not associated to the phases and were indexed, for example, as iron oxide. Figure 17(b) shows the diffractogram for the sample aged at 950 °C for 10 hours. The peaks were identified and indexed as δ-phase, (Nb,Ti)C carbide and γ-fcc matrix, according to the ASTM A936 standard which covers the procedure for the isolation of TCP in nickel-based alloys. This result confirms that the supposed Nb-rich needle-like phase is in fact a δ-phase (Ni_3Nb). Moreover, the γ'' phase could not be identified by XRD due to its small size and because it is dissolved during precipitation extraction.

The volume fraction of phases could not be quantified without information associated to the matrix because the X-ray diffraction was performed on a powder of precipitates extracted from the bulk. Therefore, in order to provide quantitative information concerning the fraction of the secondary phases precipitated into weld metal, a set of images of the weld metal using SEM in the SE mode were taken for each condition, and then

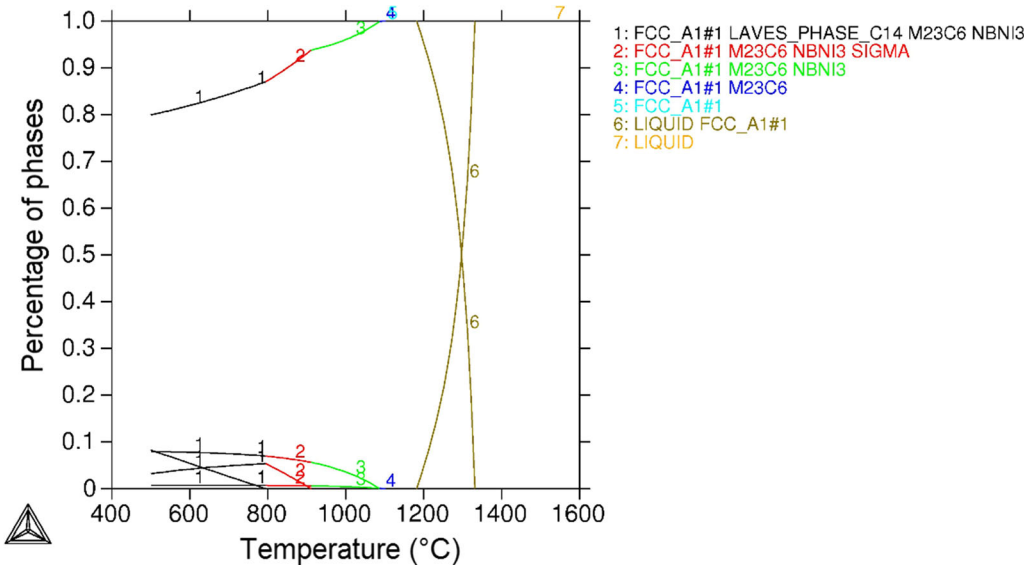

Fig. 8—Phase diagram calculated by Thermo-Calc© based on the weld metal chemical composition.

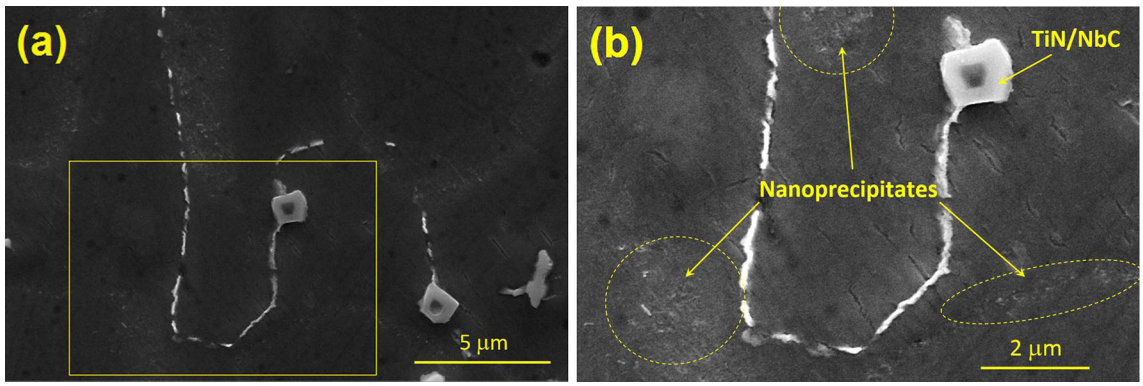

Fig. 9—Precipitation along the grain boundary and a very thin precipitation dispersed into the interdendritic region was observed, as can been more easily confirmed in the magnification (*b*) of the region indicated in (*a*).

they were evaluated using an image processing and analysis software package. This approach has been successfully used in several other studies.[22,40]

The graphs in Figure 18 show that the as-welded condition presented the greatest amount of the secondary phase. These were Laves and TiN/NbC phases, which resulted from the solidification process. This indicates the strong potential of microsegregation to form phases. When the aging time was increased to 10 hours, a decrease in the phase fraction was observed for both temperatures. This reduction with 10 hours aging at 650 °C was attributed to a partial dissolution of the Laves phase. While at the 950 °C aging temperature, the drop in phase fraction was associated to the partial transformation of Laves phase to δ-phase. Higher aging times produced a drastic drop in phase fraction that was associated to almost complete dissolution of the Laves and δ phases. The remaining precipitations observed for the 200-hour aged samples were associated to TiN/NbC cubic particles, large blocks of NbC, and some very thin carbides on the grain boundaries, possibly $M_{23}C_6$ and/or M_6C carbides. In addition, even having not been possible to quantify the amount of γ'' phase, it is important to not forget that its nucleation occurs in microstructures aged at 650 °C for the longest times (100- and 200-hour aged).

B. *Mechanical Properties Evaluation*

Figure 19 presents the results of the Charpy-V impact test. The analysis of variance (ANOVA) indicated that the absorbed energy (in joules) for both aging temperatures evaluated was significant, and varied as a function of aged time; the significance factor was below 0.00002 with a confidence of 95 pct. Table IV indicates that a high energy was absorbed for the as-welded non-aged condition (0 hour), which was higher than 140 J. For the sample aged at 650 °C, there was a slight increase in toughness, from 142 to 151 J. On prolonging the aging time, there was a noticeable drop in the absorbed energy values for the times of 100 and 200 hours. However, it is important to note that even after 200 hours of aging, the absorbed energy values were greater than 98 J. For the sample aged at 950 °C for 10

hours aging time, there was a slight decrease in toughness, with a mean value of 121 J, while the energy absorbed for prolonged aging time (100 and 200 hours) increased again.

Fractography analysis was performed on the surface of the Charpy-V impact test samples, in order to understand the details about the cracking behavior. The images were acquired using SEM operating in the SE mode. Figures 20(a) and (b) show the fractography images for the samples aged at 650 °C for 10 and 200 hours, respectively. In both cases, a ductile fracture characteristic was observed, with dimple structures.

Figures 21(a) and (b) show the fractography surface of the samples aged at 950 °C for 10 and 200 hours, respectively. As observed in the fractography images of conditions aged at 650 °C, the conditions aged at 950 °C show the same ductile fracture characteristic.

An EDS mapping was obtained from the sample aged at 950 °C for 200 hours, in order to detect the position of the secondary phases in relation with the fracture morphologies. Figure 22 shows the EDS mapping, which highlights a high concentration of Nb and Ti into the dimples core, indicating thus the presence of precipitates in that region.

The results of the microhardness test were evaluated statistically by analysis of variance (ANOVA), as shown in Figure 23. Again, the statistical analysis shows that the hardness varied with 95 pct confidence as a function of aged time, which is indicated by the significance factor below 0.00002. On evaluating the hardness curve for samples aged at 650 °C for a short period of time, no significant changes were found for the hardness, which remained at approximately 300 HV. However, increasing the exposure at high temperatures for long times such as 100 and 200 hours, the hardness values rose to 437 and 443 HV, respectively. Though, no difference in terms of hardness was found when the time of exposure was changed from 100 to 200 hours. In addition to the statistical analysis, the variation in hardness was very significant in practice, since the difference from the lower to higher values was almost 150 HV.

The hardness results obtained are in agreement with toughness behavior evaluated by the Charpy test. As shown in Figure 19, the samples aged at 650 °C for short time periods (0 and 10 hours) had an impact energy between 140 and 150 J, whereas samples aged for 100 and 200 hours experienced a drop in this property. Since the hardness remained low for short aging times and underwent an increase for long times of exposure, the behaviors of both properties are fully consistent, having a direct correlation, and indicating that a hardening mechanism took place during aging at 650 °C.

C. *Physical Properties Evaluation*

Albuquerque *et al.*,[25] presented the ultrasound velocities obtained using transducers with frequencies of 4 and 5 MHz from the as-welded and aged at temperatures of 650 °C for 10, 100, and 200 hours samples, showing that ultrasound velocity decreased with the time of the aging heat treatment between 0 (as-welded) and 100 hours, and increased from 100 to 200 hours. This behavior is similar to the results obtained by the Charpy impact test (Figure 19) and inversely proportional the results obtained for the hardness test (Figure 23). However, Albuquerque *et al.*[25] did not consider inspection by ultrasound at temperatures of 950 °C. Taking into account the importance of this aging temperature and the same experimental conditions of Albuquerque *et al.*[25], Figures 24(a) and (b) present the related results of ultrasonic velocity and attenuation, respectively. Based on these results, no significant modification of the ultrasonic measurements was established between the times of 0 and 200 hours. This behavior was completely different to that found for the microstructure, Charpy impact energy (Table IV), and hardness tests (Figure 23).

Kumar *et al.*,[41] showed that the variation in ultrasonic longitudinal wave velocity with aging time in Inconel 625 alloys exhibited similar behaviors, indicating that the change in ultrasonic velocity is associated with the change in mechanical properties due to the formation and dissolution of various precipitates.

According to the measurements for the 650 °C aged conditions, nondestructive ultrasonic testing may be a promising tool for monitoring phase changes in 625 alloys. However, based on the 950 °C aged condition, this technique was demonstrated to be sensitive to the microstructures formed. Therefore, further studies for the application of nondestructive techniques to detect microstructural changes in nickel-based alloys by ultrasound should be developed, especially since the dispersion of signals has demonstrated that this technique is sensitive to the phase type, particle size, morphology, and other features that hamper the analysis, interpretation and establishment of correlations between microstructural characteristics. Moreover, to identify the technical capabilities and limitations of these techniques, additional investigations are still necessary.

IV. DISCUSSION

A. *Microstructure*

Based on morphology and chemical composition performed by SEM-EDS analysis, the shapeless or eutectic particles were characterized as a TCP phase named Laves phase rich in Nb. These results are consistent with those reported by other authors evaluating the microstructure of 625 alloy.[13,14,42]

In addition, the presence of cubic precipitates has been reported for the 625 alloy in the literature.[42,43] In another study, Silva *et al.*[42] confirmed by TEM analysis that these cubic precipitates observed in the microstructure are a complex precipitate, consisting of a core with titanium nitride (TiN) surrounded by a niobium titanium carbide (NbTi)C.

Due to the high melting point of the NbTiN complex of carbides/nitrides (2927 °C),[44] which is approximately twice the *liquidus* temperature of the 625 alloy, it is quite likely that they remain in the solid state within

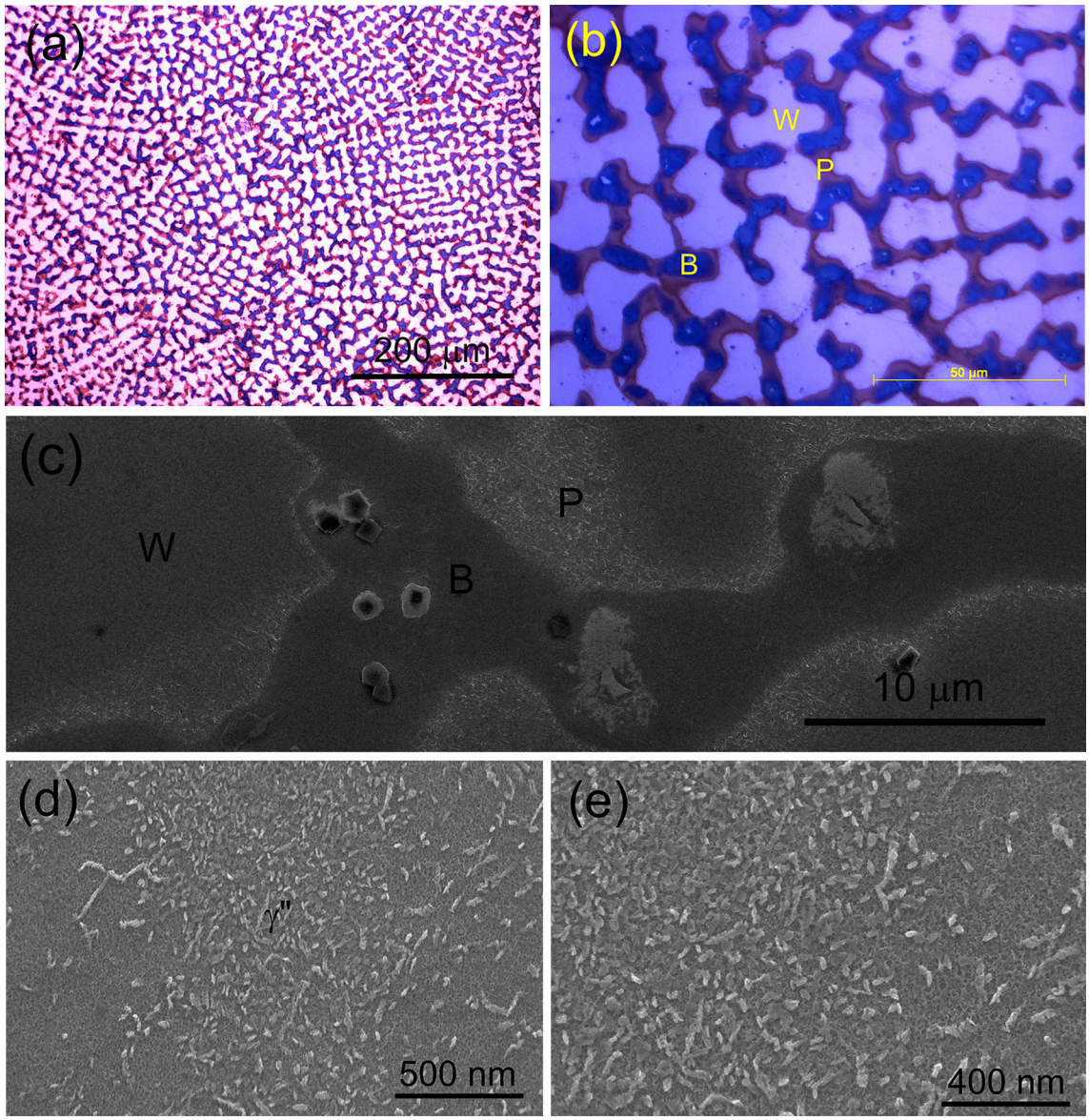

Fig. 10—Microstructural analysis performed to observe nanometric precipitation in the sample aged at 650 °C for 200 h. (*a*) Light microscopy showing a colored aspect of the microstructure after perchloric acid electrolytic etching. (*b*) LM details showing three distinct regions: white (W), purple (P), and blue (*b*). (*c*) SEM image in low magnification showing the three regions observed in LM. Heterogeneous nucleation of γ'' phase in weld metal is observed. (*d*) and (*e*) High-resolution SEM-FEG images showing intense γ'' phase precipitation along blue region observed by LM.

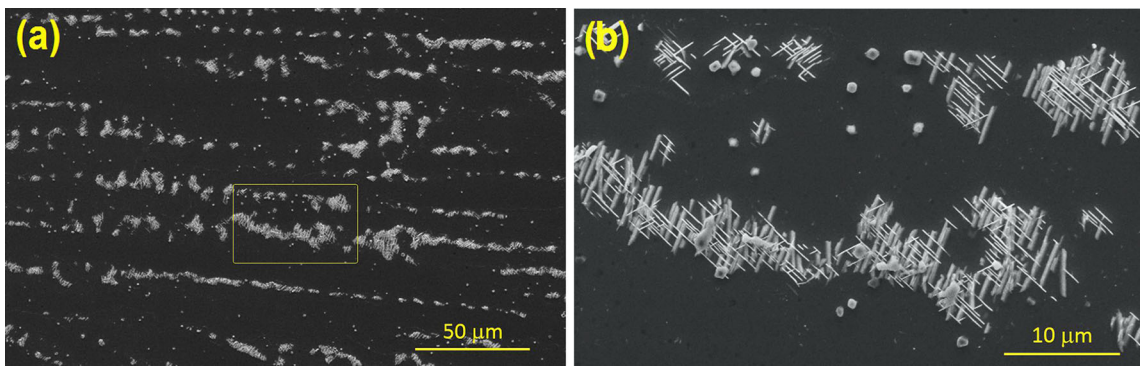

Fig. 11—(*a*) Example of SEM micrograph using secondary electrons showing the aged microstructure at 950 °C for 10 h taken from different positions. (*b*) Enlarged image from the region indicated in (a).

the volume of the liquid pool, differently of Laves phases which have a low melting point and are formed during the solidification reaction.

The microstructural evolution due to thermal aging was evaluated. The results obtained indicate the formation of a discontinuous precipitation of very thin precipitates along the grain boundaries for the sample aged at 650 °C for 100 hours, whereas for the 200 hours aging, a continuous thin film precipitate along the grain boundaries was observed.

To facilitate the understanding of the phase precipitation phenomena during thermal aging, and taking into account the overall composition of the weld metal indicated in Table I, a TTT diagram was built by the Calphad computational approach using JMatPro software, as shown in Figure 25. The results of this simulation showed that three different types of carbides can form at 650 °C, with different nucleation times. The carbide with the most favorable kinetics was $M_{23}C_6$, which initiated its nucleation and growth process at around 41 hours, and then came M_6C, which initiated its nucleation at approximately 83 hours. Finally, the carbide-type M_7C_3, which, according to the results of the simulation, precipitated only after 133 hours. These results are in agreement with several others reported in the literature. Chakravartty *et al.*[16] evaluated a tube exposed to high temperatures ranging from 650 to 680 °C after 100,000 hours in service, and reported the formation of a thin layer of discrete carbide particles at the grain boundaries, which were identified by TEM as $M_{23}C_6$ carbide. In addition, these authors found large chunky $M_{23}C_6$ carbide particles at the grain boundaries.

Evans *et al.*[45] performed a series of creep tests of foils in air at 750 °C, and among several significant changes in microstructure, the authors reported that the grain boundaries became heavily decorated with precipitates, the majority of which were rhombohedral μ phase. Additionally, a significant fraction of the grain boundary precipitates was found to be a Si-rich variant of M_6C. This suggests that the particles formed along grain boundaries are most likely to be $M_{23}C_6$ and M_6C carbides.

Additionally, the TTT diagram also presents the "C" curve to γ'' phase precipitations under isothermal treatment. According the diagram, at 650 °C temperature, the precipitation must start only after at least 100 hours. In fact, the results of SEM analysis shown that for aging as long as 200 hours, the weld microstructure has produced a heterogeneous nucleation of γ'' phase. However, in this study, the precipitation has been observed also for 100-hour aged condition. These differences in terms of starting time to nucleate the γ'' phase and the heterogeneous nucleation pattern can be attributed to the microchemical differences observed in microstructure, due to microsegregation during solidification, since the diagram was built considering a homogeneous distribution of alloying elements in microstructure.

The heterogeneous precipitation of γ'' phase has been observed in other studies. Suave *et al.*,[8] using high-resolution scanning electron microscopy identified the precipitation domains of the γ'' phase and observed a heterogeneous precipitation behavior. In addition, the authors also observed that the precipitation of γ'' particles was retarded in shear spinning samples, being hence dependent to initial microstructural condition. Past studies performed by Pai *et al.*[46] and Sundararaman *et al.*,[47] also reported that the first stages of γ'' phase precipitation were observed to be heterogeneous. Therefore, the results found in this study are in good agreement with the literature.

For the samples thermal aged at 950 °C, the microstructural analysis shows the presence of a new type of precipitate. The evaluation of the characteristics of this new phase of needle particles, and their comparison with information reported in the literature, showed that these needles are most probable an ordered phase, whose stoichiometric composition is Ni_3Nb with an orthorhombic crystallographic structure.[48,49] This phase is commonly observed in Ni-based alloys containing Nb, such as the 625 and 718 alloys, and can precipitate in a wide range of temperatures and presenting various morphologies.[50]

As mentioned before, the interdendritic region is enriched in Nb due to microsegregation during solidification, which makes the precipitation of phases rich in this element possible. In fact, based on the results presented before, the δ-phase needles are formed due to the favorable microchemistry in the dendritic region, having a high concentration of Nb, which is the main element of δ-Ni_3Nb. However, this formation is different from what has been observed for Ni-based superalloys with the addition of Nb in annealing conditions, when the δ-phase forms due to the decomposition of γ'' phase, since both phases have the same stoichiometry but different crystal structures.

According to Delueme *et al.*,[51] there are two kinds of δ-phases depending on the precipitation temperature. Phases formed in the temperature range 900 to 1000 °C are named δ_{HT} and are characterized by coarse spheroidized or platelet formations. When the δ-phase is precipitated at lower temperatures (around 750 °C) during the aging heat treatment, the phase is named δ_{LT}, and is precipitated in the form of a film or continuous strings along the grain boundaries.

Mittra *et al.*[18] suggested that lath-shaped δ-phases form in 625 alloys when they are held isothermally at 850 °C. Since, this temperature is the nose temperature of the "C" curve corresponding to the δ-phase of 625 alloys, the presence of this ordered phase is expected in all the samples.

The TTT diagram presented in Figure 25 indicates that the δ-Ni_3Nb phase cannot form at temperatures above 900 °C. However, this particular phase was observed after aging at 950 °C. In fact, there is another recent study that reported δ-Ni_3Nb phase precipitation in a 625 alloy under thermal aging at around 900 °C.[8] However, as commented there are many points to be considered in these analysis, depending on the welding conditions applied. The global chemical composition of the weld metal was taken into account to build the TTT diagram presented here, and any compositional heterogeneity, such as microsegregation, was disregarded. On the other hand, in the study performed by Suave *et al.*,[8] the material evaluated was a

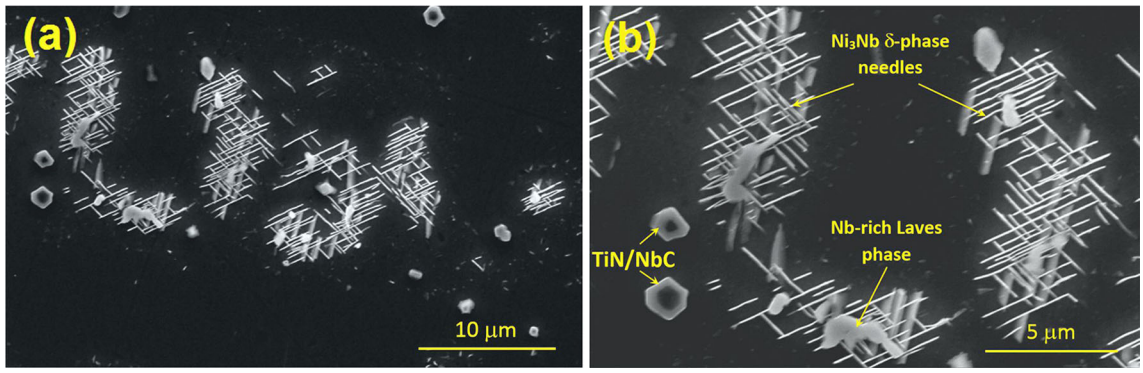

Fig. 12—(*a*) Details of TCP phases in the microstructure showing Ni_3Nb δ-phase needles together with Nb-rich Laves phases into the interdendritic region. (*b*) Additionally, a large cubic precipitate of NbTi complex carbide/nitrite was observed.

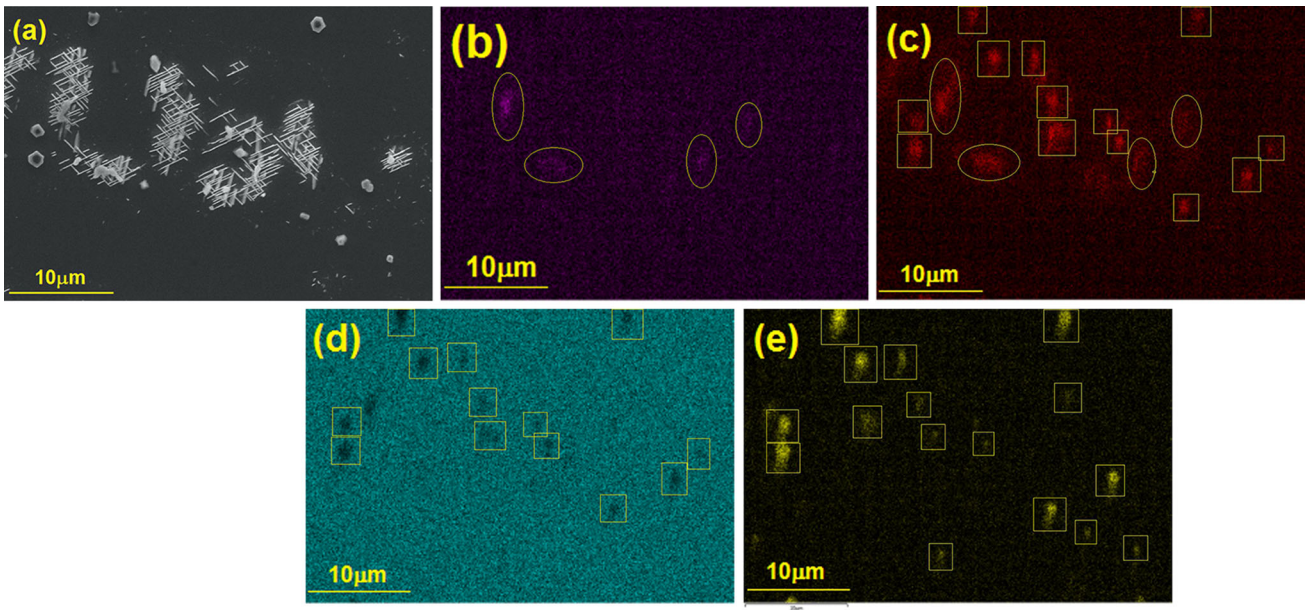

Fig. 13—Chemical mapping obtained by EDS for the alloying elements: (*a*) SEM image, (*b*) Mo, (*c*) Nb, (*d*) Ni, and (*e*) Ti.

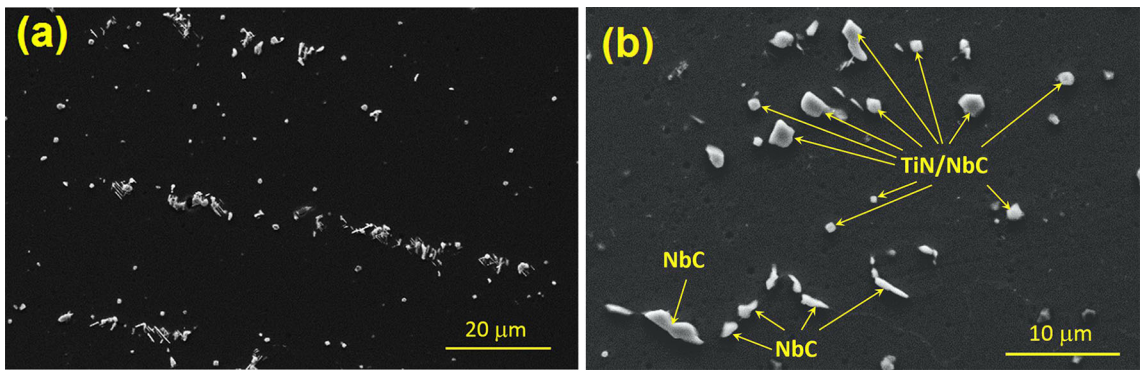

Fig. 14—(*a*) Examples of SEM micrographs using secondary electrons showing the aged microstructure at 950 °C for 100 h taken from different positions and different magnifications. (*b*) Enlarged image showing large NbC blocks.

625 alloy sheet, under two different conditions: as-rolled + solution-treated and shear spinning, which had an initial microstructure essentially formed of γ-fcc and small carbides. Thus, the experimental TTT diagram reported by these authors was obtained from an alloy with a homogeneous chemical composition.

However, in this study, it was proven that the Laves phase was formed due to microsegregation during solidification. These Laves phases, which act as a niobium reserve for the formation of the γ'' phase and δ-phase, dissolve over time, and thus supply the supposed element to the system so that there is a continuous formation of both γ'' phase and δ-phase, depending on aging temperature and time. Therefore, the kinetics of phase transformations is strongly affected by chemical heterogeneities and the initial microstructure, besides the thermal and thermomechanical history.

These results are in agreement with data reported by Floreen *et al.*,[20] who also studied the metallurgy of a 625 alloy. These authors evaluated the behavior of δ-phase precipitation by comparing a weld metal with a wrought alloy piece. Their results revealed that the field of the δ-phase is expanded if the temperature is increased up to 980 °C. In addition, the time the precipitation started in the weld metal was reduced by a factor of 50 when compared to the wrought condition.[20] Another study of 625 alloy aging in the welded condition was developed by Cortial *et al.*[52] Their analysis focused on changes in the heat treatment temperatures, maintaining the holding time at 8 hours. These authors found that at temperatures of 850 and 950 °C, there was a formation of fine needles identified by TEM as the δ-phase, corroborating with the results presented here.

B. *Mechanical Properties*

Concerning the general effect of aging treatment on mechanical properties, by evaluating the results obtained in the Charpy-V impact test for the 650 °C aged condition, it was found that energy absorbed varied as a function of aged time. As reported by Thomas and Tait,[19] the heat treatment at comparatively modest temperatures ranging from 650 °C to 700 °C and for reasonable times of 6 to 12 hours proved beneficial in regenerating the toughness of some alloys.

Notwithstanding, the behavior exhibited by the post aging material was consistent with the microstructural changes previously reported. From the as-welded sample to the 10-hour aged sample, a small dissolution of Laves phase was observed, which implicated in an increase in toughness. For longer times of exposures (100 to 200 hours), the main microstructural changes were the dissolution of Laves phase, γ'' phase precipitation in interdendritic region, and precipitation of nanometric carbides particles along the grain boundaries. If on one hand the decrease in the volume fraction of Laves phase has proved interesting to improve the impact resistance; on the other hand, the precipitation γ'' phase in interdendritic region and the precipitation of finely dispersed nanosized carbide particles along grain boundaries and sub-grain boundaries were found to be harmful to toughness (impact test).

Also for 100 and 200 hours of exposure at 650 °C, the presence of large blocks of NbC carbides and cubic NbTi complexes were found, which remained from solidification. However, these particles probably have low or no effect on toughness, since these particles were found in another study, carried out by Silva *et al.*[53] evaluating the effect of the interpass temperature on mechanical properties in the weld metal of 625 alloys. The results of Charpy-V impact test at cryogenic temperature (-196 °C) showed no significant differences among the weld conditions and the level of energy absorbed was higher than 100 J. Therefore, it is believed that the harmful effect on impact strength was due to the intense precipitation of γ'' phase in interdendritic region, and of carbides along the grain boundaries.

The fractographic images of the conditions aged at 650 °C showed that the changes in toughness were not reflected in the fractography behavior. The ductile characteristic observed in the recovered condition aged for 10 hours was the same noted for the worst toughness condition, which was aged for a long period of exposure (200 hours).

The results of the microhardness tests were also evaluated and they were statistically significant, and varied as a function of aged time. Thomas and Tait[19] evaluated the hardness of an aged 625 alloy and found 230 HV_{30} for annealed material conditions, while for samples aged at 650 °C after 3, 6, and 12 hours resulted in hardness values ranging from 303 to 317 HV_{30}. In fact, the 10-hour aged sample achieved hardness similar to that found by Thomas and Tait[19] for aged materials (300 HV). Nonetheless, the materials studied were not weld metals; therefore, the initial precipitation of Laves phase due to solidification would probably make the hardness higher if compared to annealing conditions. In addition, the authors reported that the results of hardness for a pipe that had been in service for approximately 50,000 hours at 500 °C, a value of 444 HV_{30} was found. Kirman and Warrington[54] also reported that the aged material at 650 °C achieved a peak hardness of 400 HV after about 500 hours of aging. Therefore, the hardness values measured for samples aged at 650 °C for the higher exposure times evaluated in this study (100 and 200 hours) are in agreement with those in the literature.

The reason that may possibly cause the increase in hardness was observed by the high-resolution scanning electron microscopic technique used in this study. The main microstructural changes able to produce the increase in hardness are the precipitation of the γ'' (Ni_3Nb) phase, which was found for the higher exposure times (100 and 200 hours). According to the TTT diagram (Figure 25), the γ'' phase is able to form at 650 °C. Several studies in the literature have reported the formation of γ'' at this temperature.[8,20,39]

Precipitation of the γ'' phase in Ni-based alloys is responsible for a strengthening mechanism, which improves the room- and high-temperature mechanical properties, including tensile strength and hardness.[8,20,39,45,55–57] Therefore, the precipitation of this particular phase is well established and its formation together with Laves and delta-phases under the aged conditions ranging from 600 °C to 900 °C.[58–62] Consequently, as previously mentioned, the intense precipitation of γ'' phase along the interdendritic region in microstructure may would justify the observed increase in hardness.

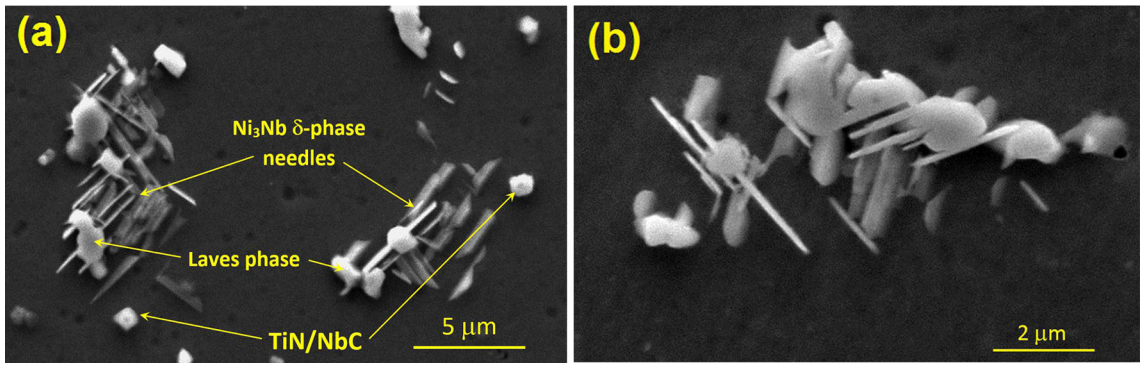

Fig. 15—(*a*) Example of microstructure of the sample aged at 950 °C for 100 h. (*b*) In detail, some secondary phases formed by Laves phase not dissolved, δ-phase Ni_3Nb needle-like and some NbTi carbide/nitride cuboidal particles.

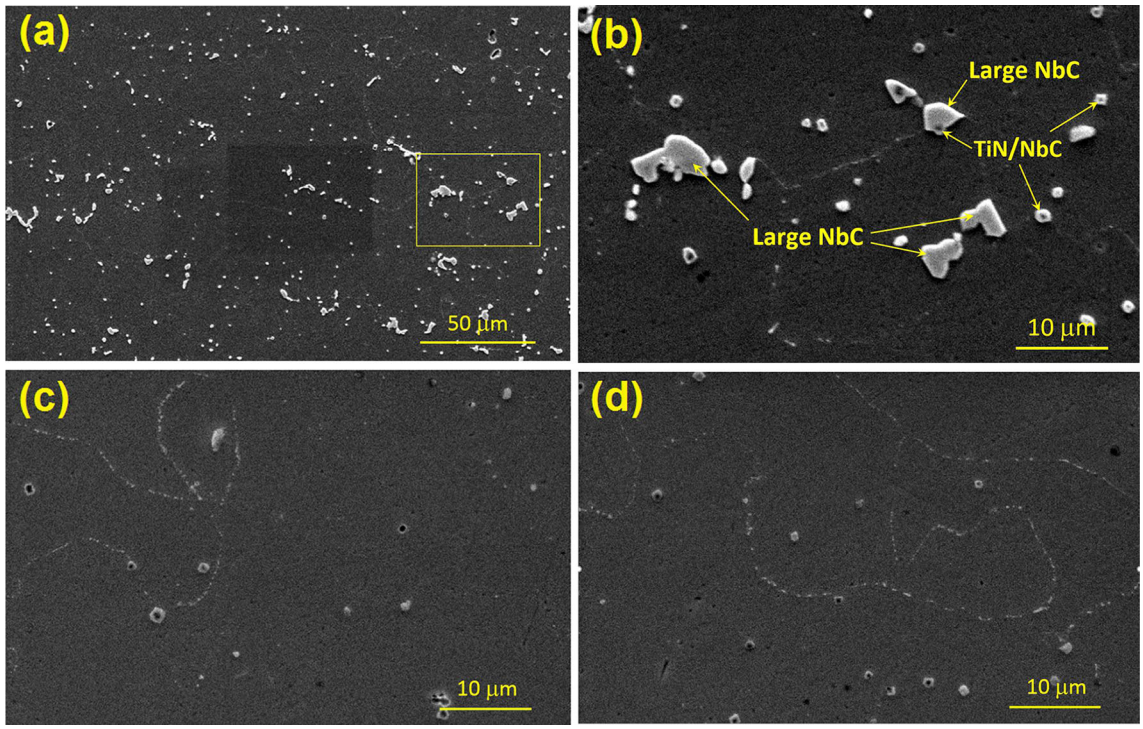

Fig. 16—Examples of SEM micrographs using secondary electrons showing the aged microstructure at 950 °C for 200 h taken from different positions: (*a*) and (*b*), regions showing cubic NbTi carbides/nitrides and large NbC carbides; (*c*) and (*d*), Small cubic NbTi carbides/nitrides and a fine precipitation at the grain boundaries are perceived.

Concerning the general effect of aging treatment on mechanical properties for 950 °C aged condition, the literature reports that the formation of the δ-phase in significant quantities can be harmful to the mechanical properties for precipitation hardening Ni-based alloys.[63] In the case of the 625 alloy, which is a solid-solution strengthened alloy, the precipitation of δ-phase is produced after long time exposure at high temperatures from the solid solution supersaturated. Precipitation of δ-phase leads to reduced ductility.[64]

Another study showed that both hardness and tensile strength decreased with an increase in aging temperatures due to the precipitation and coarsening of the delta-phase.[58] Therefore, the drop of impact energy absorbed by the sample after a 10-hour treatment at 950 °C suggests that the precipitation of the δ-phase in the weld metal of a 625 alloy aged at 950 °C found in this study has a harmful effect on the mechanical properties of the alloy.

The detailed microscopic analysis performed for samples thermal aged at 950 °C showed that many particles remain in microstructure even for long exposure times. This behavior indicates that the aging conditions (time and temperature) were not favorable to dissolve completely the TCP phases. Cai *et al.*,[59] studied the dissolution kinetics of δ-phase in a 718 alloy, which has additional Nb, and mentions that the δ-phase can be fully dissolved into the matrix after a heat treatment at 1020 °C for more than 2 hours. However, when held at 980 and 1000 °C, a certain amount of

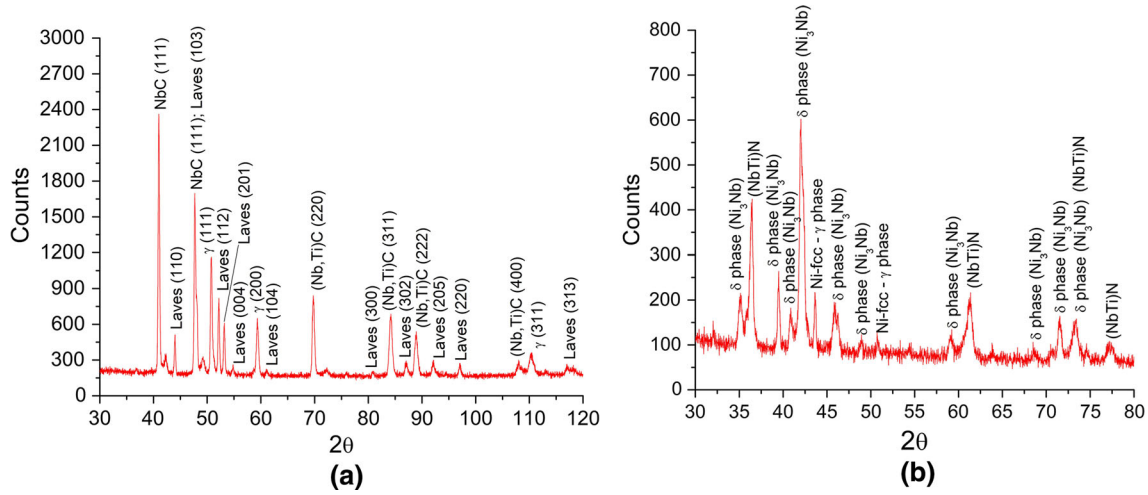

Fig. 17—X-ray diffractograms from powder extraction concentrated in the secondary phases: (*a*) sample aged at 650 °C for 10 h; and (*b*) sample aged at 950 °C for 10 h.

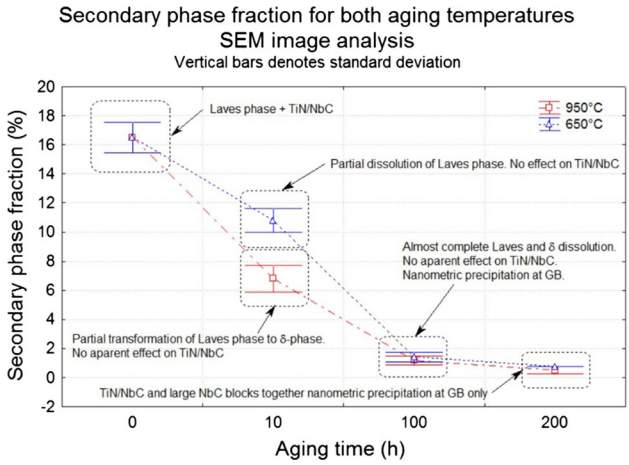

Fig. 18—Quantitative analysis of secondary phase fraction in weld metal carried out by SEM image analysis.

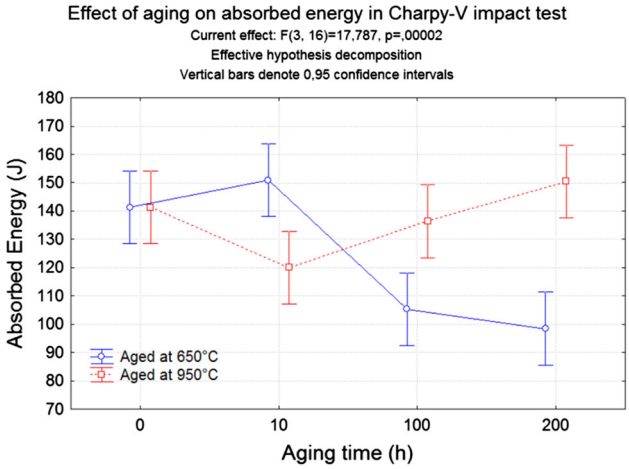

Fig. 19—Results of the effect of aging temperature and time on the absorbed energy in the Charpy-V impact test, evaluated by analysis of variance.

δ-phase was still found in the alloy, even after more than 6 hours. In this case, the chemical inhomogeneity due to microsegregation and the formation of Nb-rich phases during solidification makes the precipitation and dissolution kinetics of the δ-phase different in 625 nickel-based weld metals.

Xing *et al.*[60] evaluated the effect of post-weld heat treatment temperature on the microstructure of an Inconel 625 alloy and found that at 950 °C, the δ-phase disappeared, similar to the behavior observed in this study. In addition, these authors reported that small amounts of blocky secondary phases appeared at the grain boundaries, which were identified by TEM analysis as M_6C-type carbide, with a face-centered cubic (fcc) structure and lattice parameter of 1.12 nm. Thomas and Tait[19] also reported some precipitates at grain boundaries. The EDS analysis of those particles indicated that they were rich in molybdenum and niobium, which has led these authors to conclude that they were carbides of the M_6C type. Similar results were found by Ferrer *et al.*[61] and Burke and Miller.[62] This reinforces the suspicions that the thin precipitation along the grain boundaries are particles of M_6C carbides.

In addition, the results obtained by XRD analysis were consistent with the ones reported in the literature.[65] This result confirms that most probably the whole volume of Laves phase was consumed during the aging treatment, providing the niobium necessary for the formation of the δ-phase. This behavior is in agreement with the microstructural observations performed by SEM in this study.

For the conditions aged at 950 °C, a different behavior was observed. There was a significant drop in fracture toughness for the sample with 10 hours of treatment, as previously mentioned. Then, there was an increasing in toughness over time, returning to about the same level as the as-welded condition. This drop in the impact strength for the sample of 950 °C and 10 hours was attributed to the precipitation of the delta-phase

Table IV. Impact Strength of As-Welded and Aged Condition Obtained by the Charpy-V Impact Test

Sample	Impact Strength (J)
As-Welded (0 h)	141.3 ± 14.3
650 °C/10 h	150.9 ± 6.8
650 °C/100 h	105.3 ± 3.3
650 °C/200 h	98.4 ± 1.2
950 °C/10 h	120.0 ± 3.7
950 °C/100 h	136.4 ± 6.9
950 °C/200 h	150.4 ± 5.5

needles in interdendritic regions. This indicates a detrimental effect of precipitation. For 100 hours of treatment at 950 °C, there was a significant reduction in the amount of delta-phase, which resulted in a recovery of the impact resistance. For 200 hours of treatment, as reported above, a microstructure consisting of only large blocks of Nb carbides and cubic precipitates of NbTi carbides/nitrides was found.

Although nanometric precipitation along the grain boundaries and sub-grain boundaries has been reported for 950 °C aging treatment, this was less intense compared to those observed for aging at 650 °C. Therefore, the results of impact resistance indicate that this microstructural condition was not detrimental to the weld properties.

According Mittra *et al.*,[18] the ductility of 625 alloy after 1200 hours of aging at 540 °C (813 K) is seen to be much higher than that of all samples aged at 973 K (700 °C) and 1123 K (850 °C). The formation of large plate-shaped δ phases at 1123 K (850 °C) results in lower strength and ductility compared to that of 973 K (700 °C). A considerable amount of δ formation after 1200 hours of isothermal holding is also seen to produce {111} plane facets. However, fine micro-dimples of uniform size are seen along the facets of the fractograph. Since the ductility and toughness of the Ni-fcc matrix are very high, the reduction in impact strength was lower than expected for aged conditions, but its influence was enough to observe the behavior that was directly linked with the microstructural changes.

Thomas and Tait[19] confirmed that the improvement in properties after heat treatment at 650 to 700 °C was most successful for the recovery of some toughness as observed in the as-received material. However, the toughness still remained low compared to as-received material. It is possible that this was due to the formation of orthorhombic δ phase. Another work[56] found that a reduction in Charpy impact energy to around 180 to J/cm^2 occurred as a result of intermediate temperature aging, which was attributed primarily to the formation of the orthorhombic δ phase.

The fracture surface analysis of conditions aged at 950 °C showed a ductile fracture, even for 10 hours of treatment that shows the lowest impact toughness. According to Mittra *et al.*,[18] in most cases the heat treatment performed on Inconel 625 alloy affects its microstructure. However, the nickel matrix maintains the ductile fracture characteristic even for significant changes in the microstructure.

As referred to previously, the fractographic images indicate the presence of some small particles in the dimple cavities. In addition, the fracture features reveled some similarity with the microstructure, in which the crack propagation pattern and dimples were aligned along a specific direction (Figures 20(b) and 21(a)), similar to the dendrite growth orientation assumed during solidification.

Moreover, the fractograph shows that the precipitates are located in dimples. This suggests that the interdendritic regions observed in the microstructure, which is decorated with precipitates, are the preferable regions to open the cavities under stress. In this case, the precipitates acted as pinning points, blocking the movement of dislocations and preventing the plastic deformation of the Ni matrix, which is in accordance with the suggestion made by Sheng *et al.*[65] On the other hand, the dendrite core regions are precipitate free and show a decrease in the solid solution elements such as Mo, Nb, and Ti. Consequently, lower mechanical strengthening due to both factors, lower solid solution and the absence of precipitates, will improve the ductility of the dendrites formed by a γ-fcc matrix, when compared with the interdendritic regions, which, due to the microsegregation phenomena, cause a heterogeneous chemical composition and phase precipitation.[42]

The EDS mapping performed on the fracture surface of the sample aged at 950 °C for 200 hours (Figure 22) highlighted the presence of Nb-rich carbides and the cubic precipitates of NbTi carbides/nitrides which were located mainly in the dimple cores. This reinforces the assumption that these precipitates acted as pinning points to block the dislocation movements, thus giving support to the hypothesis proposed to justify the fracture behavior.

Thus, the fracture surface can be correlated with the microstructure, assuming that the dimples arise from small precipitates into the interdendritic regions, and the dendrite core, which is precipitate freely, is necked and sheared during further yielding.

Considering the samples aged at 950 °C, the hardness measures increased continuously from 0 to 100 hours, going up from 291 HV (0 hours) to 395 HV (10 hours) and 469 HV for aging times of 100 hours. However, on increasing the aging time to 200 hours, the hardness decreased to 422 HV. This behavior shows that intense δ-Ni_3Nb phase precipitation after 10 hours of exposure produces an increment of 100 HV approximately, compared to the as-welded condition (0 hours).

Nevertheless, the maximum value of hardness was achieved when the 625 alloy weld metal was exposed to 950 °C for 100 hours. For this particular condition, the microstructure shows a reduction in the amount of δ-phase precipitated, growth of NbC blocks, and a nanometric precipitation around δ-phase island within interdendritic region, as well as along grain boundary and sub-grain boundary. Also for 200 hours of exposure, the hardness value does not change significantly, even experiencing an expressive microstructural variation, denoted by a complete delta-phase dissolution, growth of large blocks of NbC particles, and nucleation of nanometric particles precipitated along grain and

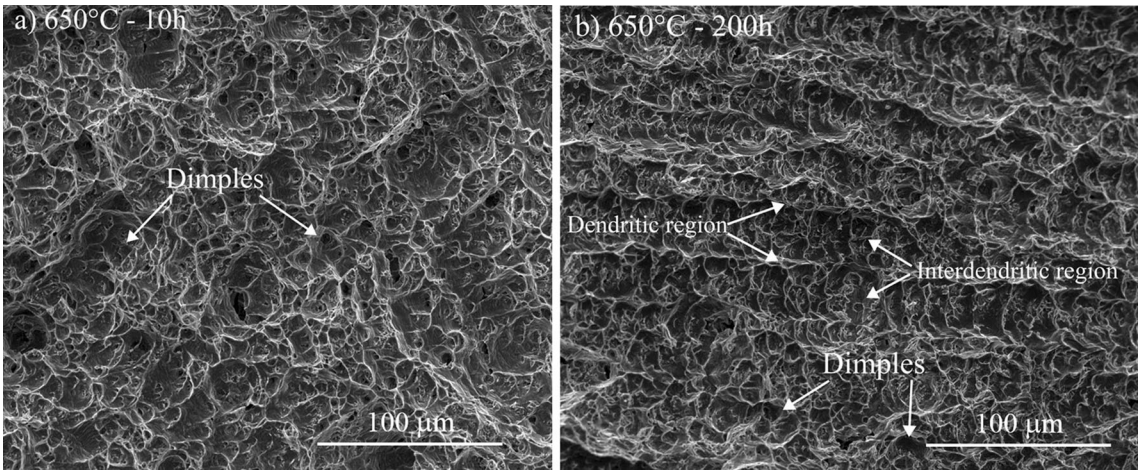

Fig. 20—Fractography images of the conditions at 650 °C for (*a*) 10 and (*b*) 200 h.

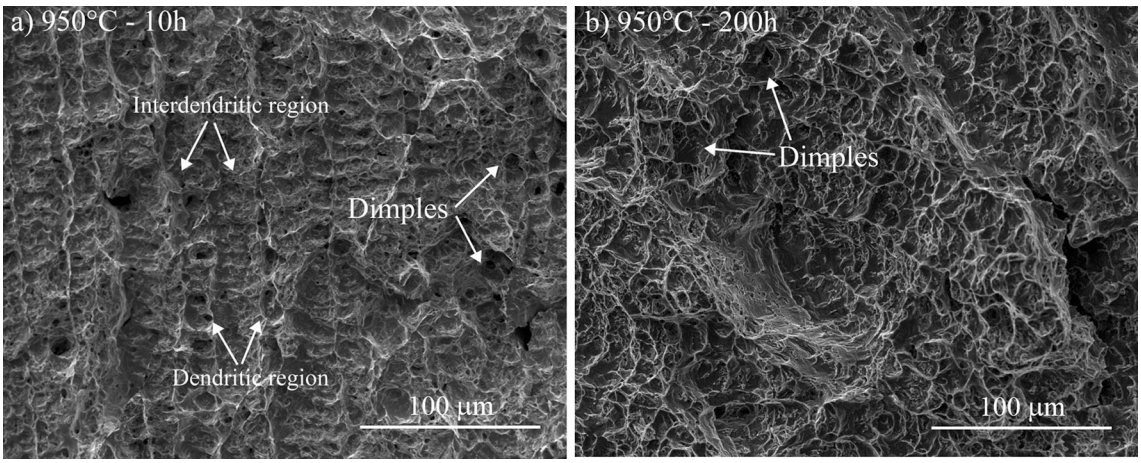

Fig. 21—Fractography images of the conditions at 950 °C for (*a*) 10 and (*b*) 200 h.

sub-grain boundaries, according to SEM analysis. Thus, it is probable that the different kinds of secondary phases ranging from micrometric to nanometric sizes, such as TiN/NbC cubic complex carbides-nitrides, large NbC blocks, δ-phase needles, nanometric carbides and, also, any solid-solution effect, must have been responsible to a strengthening mechanism, acting as pinning point to dislocation slip, causing the increase in hardness. This assumption is in good agreement with some recent studies which have reported a strengthening provided by the δ precipitation.[66,67]

The hardness and the toughness results obtained in the Charpy-V impact test showed that the δ-phase, whose precipitation was quite intense with an embrittlement effect denoted by a drop in impact resistance, did not cause any significant effect on hardness. On the other hand, for the condition of maximum hardness in the treatment of 950 °C (100 hours), the microstructure had a very small amount of delta-phase and experienced a higher impact resistance compared to the 10-hour aged condition. A similar behavior was reported by Cortial *et al.*[52] for impact toughness at the 600 to 750 °C aging temperature range. However, these authors did not report any alteration in terms of hardness. On the other hand, the time of exposure at the high temperatures in this case was shorter than that used in this study. Thereby, it was not possible to establish a direct correlation between hardness and impact resistance for the 625 alloy aged at 950 °C. Further studies must be performed to understand this behavior.

V. CONCLUSIONS

Based on the results obtained experimentally in this study for the effect of aging temperature and exposure time on the microstructure and mechanical properties of a 625 alloy weld metal, the following conclusions can be made:

(1) The microstructural evolution at 650 °C revealed that Laves phase rich in Nb produced by microsegregation during solidification was continuously dissolved with the increase of exposure time, an intense precipitation of nanosized particles along the grain boundaries was observed, and

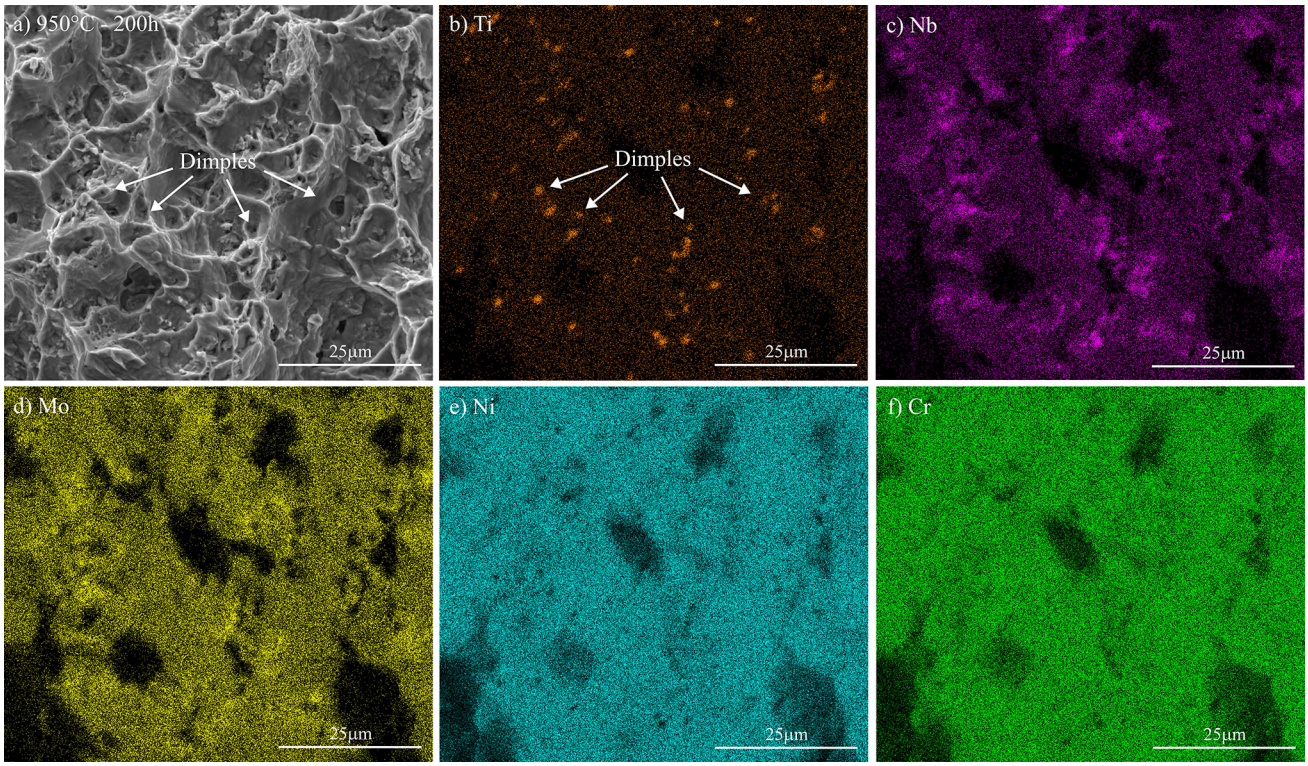

Fig. 22—EDS mapping of the condition aged at 950 °C for 200 h: (*a*) Fracture surface image and the respective chemical mapping of the elements: (*b*) Ti, (*c*) Nb, (*d*) Mo, (*e*) Ni, and (*f*) Cr.

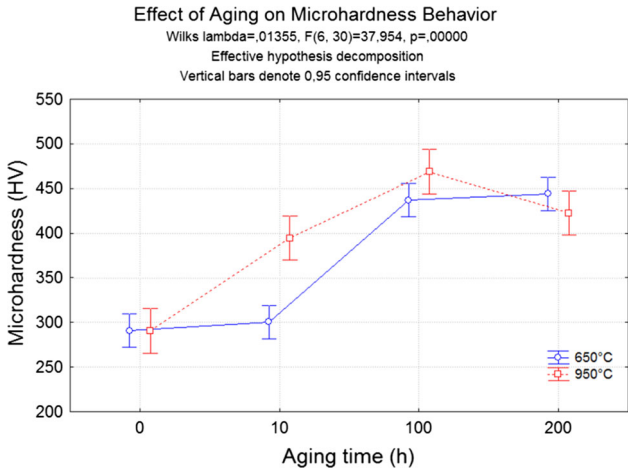

Fig. 23—Results of the effect of aging temperature and time on the microhardness Vickers test assessed by analysis of variance.

γ'' phases precipitated in interdendritic region for long periods of exposure, over 100 hours. For the TiNb complex carbides/nitrides found in the as-welded condition, no change was observed.

(2) For the aging temperature of 950 °C for a short exposure time, there was an intense precipitation of Ni_3Nb δ-phases along the interdendritic region, and Laves phase was partially dissolved and replaced by δ-phases. For the longest exposure times, δ-phases were completely dissolved, and only TiNb complex carbides/nitrides remained together with a very fine precipitation along the γ-fcc matrix grain boundaries.

(3) In terms of the Charpy-V impact test results, the energy absorbed for the 0 and 10 hours samples aged at 650 °C was kept almost the same; however, there was a decrease for the longer exposure times such as 100 and 200 hours. When the aging temperature was increased to 950 °C, the impact energy absorbed fell at 10 hours exposure, but increased for longer exposure times. The impact energy values achieved were regarded as very good, and in general were higher than 100 J.

(4) The aging effect at 650 °C on the hardness behavior showed a good correlation with the response of impact resistance, since when there was an increment in hardness there was a drop in the impact energy absorbed. The same behavior was not found for the treatment at 950 °C, in which the lower impact energy did not correspond to the maximum hardness condition.

(5) The nondestructive techniques for detection of microstructural changes in nickel-based alloys based on ultrasound signals were not able to identify the microstructural changes for the temperature of 950 °C, but demonstrated to be very promising for monitoring phase changes in

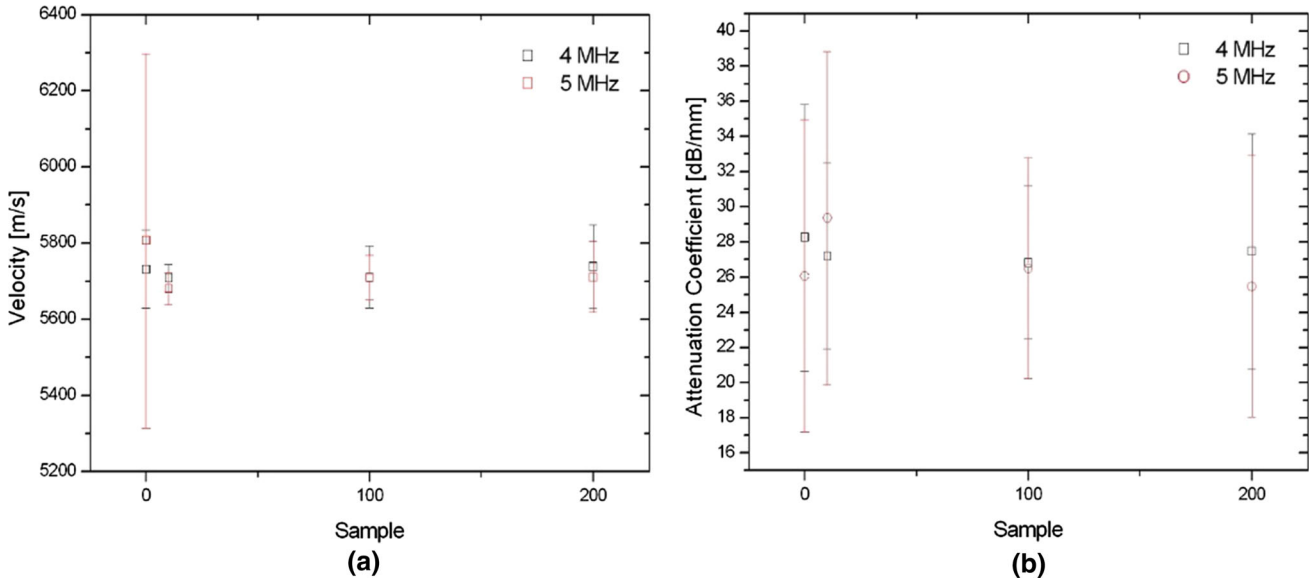

Fig. 24—Ultrasonic velocity (*a*) and attenuation (*b*) measurements obtained from samples aged for 0, 100, and 200 h.

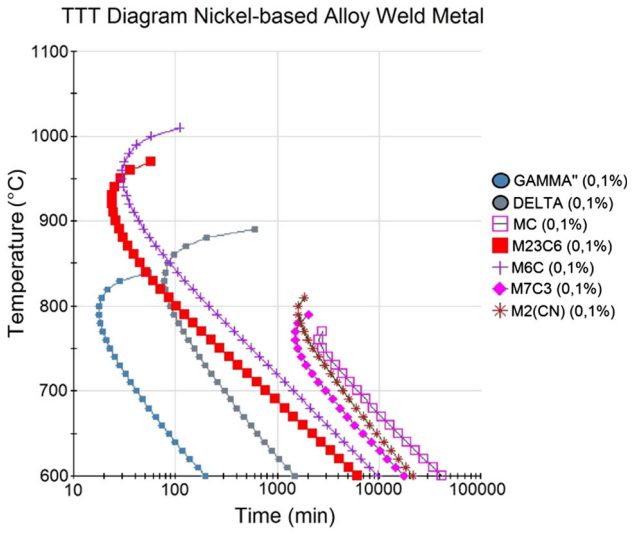

Fig. 25—Time Temperature Transformation (TTT) diagram simulated for the weld metal composition.

nickel-based alloys for aging temperatures below 650 °C. Thus, further studies are required to identify the technical capabilities and limitations for temperatures above 650 °C.

ACKNOWLEDGMENTS

The authors are grateful for the support given by the following laboratories of the Federal University of Ceará, in Brazil: Welding Research & Technology Laboratory (LPTS-UFC), Materials Characterization Laboratory (LACAM), Center of Non-Destructive Testing (CENDE), X-ray Diffraction Laboratory (LRX-UFC), Analytical Central - UFC/CT-INFRA/MCTI-SISNANO/Pró-Equipamentos CAPES. The authors would also like to thank the financial support given by National Council for Research and Development (CNPq), Research and Projects Financing (FINEP), Coordination for the Improvement of People with Higher Education (CAPES) and, finally, Petróleo Brasileiro S/A (Petrobras), in Brazil. Victor Hugo C. de Albuquerque received support from CNPq *via* the grants with reference #470501/2013-8 and #301928/2014-2. João Manuel R.S. Tavares gratefully acknowledges the funding of Project NORTE-01-0145-FEDER-000022 - SciTech - Science and Technology for Competitive and Sustainable Industries, cofinanced by "Programa Operacional Regional do Norte" (NORTE2020), through "Fundo Europeu de Desenvolvimento Regional" (FEDER).

REFERENCES

1. F.G. Hodge: *JOM*, 2006, vol. 58, pp. 28–31.
2. C.T. Sims, N.S. Stoloff, and W.C. Hagel: *Superalloys II*, Wiley, New York, 1987.
3. J.N. Dupont, S. Babu, and S. Liu: *Metall. Mater. Trans. A*, 2016, vol. 44A, pp. 3385–3410.
4. P.M. Mignanelli, N.G. Jones, K.M. Perkins, M.C. Hardy, and H.J. Stone: *Mater. Sci. Eng. A*, 2015, vol. 621, pp. 265–71.
5. E.M. Miná, Y.C. da Silva, J. Dille, and C.C. Silva: *Metall. Mater. Trans. A*, 2016, vol. 47A, pp. 6138–47.
6. M. Sundararaman, L. Kumar, G. Eswara Prasad, P. Mukhopadhyay, and S. Banerjee: *Metall. Mater. Trans. A*, 1999, vol. 30A, pp. 41–52.
7. S.S. Hosseono, S. Nategh, and A.A. Ekrami: *J. Alloys Compd.*, 2012, vol. 512, pp. 340–50.
8. L.M. Suave, J. Cormier, P. Villechaise, A. Soula, Z. Hervier, D. Bertheau, and J. Laigo: *Metall. Mater. Trans. A*, 2014, vol. 45A, pp. 2963–82.
9. Y.J. Zhang, Y.J. Huang, L. Yang, and J.G. Li: *J. Alloys Compd.*, 2013, vol. 570, pp. 70–75.
10. C.C. Silva, C.R.M. Afonso, A.J. Ramirez, M.F. Motta, H.C. Miranda, and J.P. Farias: *J. Alloys Compd.*, 2016, vol. 684, pp. 628–42.
11. D. Verdi, M.A. Garrido, C.J. Múnez, and P. Poza: *Mater. Des.*, 2015, vol. 67, pp. 20–27.
12. T.E. Abioye, D.G. McCartney, and A.T. Clare: *J. Mater. Process. Technol.*, 2015, vol. 217, pp. 232–40.

13. J.N. Dupont: *Metall. Mater. Trans. A*, 1996, vol. 27A, pp. 3612–20.
14. M.J. Cieslak, T.J. Headley, T. Kollie, and A.D. Romig: *Metall Trans A*, 1988, vol. 19A, pp. 2319–31.
15. J.N. DuPont, C.V. Robino, J.R. Michael, M.R. Notis, and A.R. Marder: *Metall Mater Trans A*, 1998, vol. 29A, pp. 2785–96.
16. J.K. Chakravartty, J.B. Singh, and M. Sundararaman: *Mater. Sci. Technol.*, 2012, vol. 28, pp. 702–10.
17. P. Liu and J.O. Nilsson: *Mater. Sci. Technol.*, 1990, vol. 6, pp. 764–71.
18. J. Mittra, S. Banerjee, R. Tewari, and G.K. Dey: *Mater. Sci. Eng. A.*, 2013, vol. 574, pp. 86–93.
19. C. Thomas, P. Tait: Int. J. Press. Vessels Pip.: 1994, vol. 59, pp. 41–49.
20. S. Floreen, G.E. Fuch, and W.J. Yang: in *Superalloys 718, 625, 706 and various derivatives*, E.A. Loria, ed., TMS, Warrendale, 1994, pp. 13–37.
21. J.J. Schirra, R.H. Caless, and R.W. Hatala: in *Superalloys 718, 625, 706 and various derivatives*, E.A. Loria, ed., TMS, Warrendale, 1991, pp. 375–88.
22. V.H.C. Albuquerque, C.C. Silva, T.I.S. Menezes, J.P. Farias, and J.M.R.S. Tavares: *Microsc. Res. Tech.*, 2011, vol. 74, pp. 36–46.
23. V.L.A. Freitas, V.H.C. Albuquerque, E.M. Silva, A.A. Silva, and J.M.R.S. Tavares: *Mater. Sci. Eng. A*, 2010, vol. 527, pp. 4431–37.
24. E.M. Silva, V.H.C. Albuquerque, J.P. Leite, A.C.G. Varela, E.P. Moura, and J.M.R.S. Tavares: *Mater. Sci. Eng. A*, 2009, vol. 516, pp. 126–30.
25. V.H.C. Albuquerque, C.C. Silva, P.G. Normando, E.P. Moura, and J.M.R.S. Tavares: *Mater. Des.*, 2012, vol. 36, pp. 37–47.
26. T.M. Nunes, V.H.C. Albuquerque, J.P. Papa, C.C. Silva, P.G. Normando, E.P. Moura, and J.M.R.S. Tavares: *Expert Syst. Appl.*, 2013, vol. 40, pp. 3096–3105.
27. VHC Albuquerque, CV Barbosa, CC Silva, EP Moura, PP Rebouças Filho, JP Papa, and JMRS Tavares: *Sensors*, 2015, vol. 15, pp. 12474–49.
28. F.E. Silva, F.N.C. Freitas, H.F.G. Abreu, L.L. Gonçalves, E.P. Moura, and M.R. Silva: *J. Mater. Sci.*, 2011, vol. 46, pp. 3282–90.
29. E.M. Silva, J.P. Leite, F.A. França Neto, W.M.L. Fialho, V.H.C. Albuquerque, and J.M.R.S. Tavares: *J. Test. Eval.*, 2016, vol. 44, pp. 2003–13.
30. V. Shankar, K.B.S. Rao, and S.L. Mannan: *J. Nucl. Mater.*, 2001, vol. 288, pp. 222–32.
31. A. Mostafaei, E.L. Stevens, E.T. Hughes, S.D. Biery, C. Hilla, and M. Chmielus: *Mater. Des.*, 2016, vol. 111, pp. 482–91.
32. Ö. Özgün, H.Ö. Gülsoy, R. Yilmaz, and F. Findik: *J. Alloys Compd.*, 2013, vol. 546, pp. 192–207.
33. E.A. Lass, M.R. Stoudt, M.E. Williams, M.B. Katz, L.E. Levine, T.Q. Phan, T.H. Gnaeupel-Herold, and D.S. Ng: *Metall. Mater. Trans. A*, 2017, vol. 48A, pp. 5547–58.
34. E Mohammadi Zahrani and AM Alfantazi: *Metall. Mater. Trans. A*, 2013, vol. 44A, pp. 4671–99.
35. D.H. Bechetti, J.N. DuPont, J.J. de Barbadillo, B.A. Baker, and M. Watanabe: *Metall. Mater. Trans. A*, 2015, vol. 46A, pp. 739–55.
36. P.G. Normando, E.P. Moura, J.A. Souza, S.S.M. Tavares, and L.R. Padovese: *Mater. Sci. Eng. A*, 2010, vol. 527, pp. 2886–91.
37. ASNT 147/147WCD, Nondestructive Testing Handbook, 3rd ed., vol. 7, Ultrasonic Testing, American Society for Nondestructive Testing, 2007.
38. *Superalloys II*, 1st ed., C.T. Sims, and N.S. Stoloff, and W.C. Hagel, eds., *Superalloys II*, Wiley, New York, 1987.
39. M. Sundararaman, L. Kumar, G. Eswara Prasad, P. Mukhopadhyay, and S. Banerjee: *Metall. Mater. Trans. A*, 1999, vol. 30A, pp. 41–52.
40. E.M. Miná, Y.C. Silva, J. Dille, M.F. Motta, H.C. Miranda, and C.C. Silva: *Mater. Charact.*, 2017, vol. 133, pp. 10–16.
41. A. Kumar, V. Shankar, T. Jayakumar, K.B.S. Rao, and B. Raj: *Philos. Mag. A*, 2002, vol. 82, pp. 2529–45.
42. C.C. Silva, H.C. Miranda, M.F. Motta, J.P. Farias, C.R.M. Afonso, and A.J. Ramirez: *J. Mater. Res. Technol.*, 2013, vol. 2, pp. 228–37.
43. C.C. Silva, C.R.M. Afonso, A.J. Ramirez, M.F. Motta, H.C. Miranda, and J.P. Farias: *Sold. Insp.*, 2012, vol. 17, pp. 251–63.
44. W Lengauer:Transition metal carbides, nitrides and carbonitrides in *Handbook of Ceramic Hard Materials*, R Riedel, ed., Wiley, Weinheim, 2000, vol. 1, pp. 202–52.
45. N.D. Evans, P.J. Mazias, J.P. Shingledecker, and Y. Yamamoto: *Mater. Sci. Eng. A*, 2008, vol. 498, pp. 412–20.
46. M. Sundararaman, R. Kishore, and P. Mukhopadhyay: in *Superalloys 718, 625, 706 and Various Derivatives*, E.A. Loria, ed., TMS, Pittsburgh, 1994, pp. 405–17.
47. H.C. Pai and M. Sundararaman: in *Superalloys 718, 625, 706 and Derivatives*, E.A. Loria, ed., TMS, Pittsburgh, 2005, pp. 487–95.
48. M. Sundararaman, P. Mukhopadhyay, and S. Banerjee: *Metall. Mater. Trans. A*, 1988, vol. 19A, pp. 453–65.
49. S.H. Zhang, H.-Y. Zhang, and M. Cheng: *Mater. Sci. Eng. A*, 2011, vol. 528, pp. 6253–58.
50. N. Kashaev, M. Horstmann, V. Ventzke, S. Riekehr, and N. Huber: *J. Mater. Res. Tech.*, 2013, vol. 2, pp. 43–47.
51. J. Deleume, J.-M. Cloué, and E. Andrieu: *J. Nucl. Mater*, 2008, vol. 382, pp. 70–75.
52. F. Cortial, J.M. Corrieu, and C. Vernot-Loier: *Metall. Mater. Trans. A.*, 1995, vol. 26A, pp. 1273–86.
53. C.C. Silva, H.C. Miranda, M.F. Motta, D.C.F. Ferreira, R.R. Marinho, and G. Dalpiaz: *Mater. Sci. Forum*, 2014, vols. 783–786, pp. 2816–21.
54. I. Kirman and D.H. Warrington: *Metall. Mater. Trans. A.*, 1970, vol. 10A, pp. 2667–75.
55. V. Shankar, M. Valsan, K. Bhanu, S. Rao, and SL Mannan: *Scripta Mater.*, 2001, vol. 44, pp. 2703–11.
56. M. Kohler: in *Superalloys 718, 612 and Various Derivatives,* E. A. Loria, ed., TMS, Warrendale, 1991.
57. A. Kumar, V. Shankar, T. Jayakumar, K.B.S. Rao, and B. Raj: *Proceedings of the European Conference in Nondestructive Testing*, J. Serrano, ed., Barcelona, Spain, 2002.
58. M.D. Mathew, K. Bhanu, S. Rao, and SL Mannan: *Mater. Sci. Eng. A*, 2004, vol. 372, pp. 327–33.
59. D. Cai, W. Zhang, P. Nie, W. Liu, and M. Yao: *Mater. Charact.*, 2007, vol. 58, pp. 220–25.
60. X. Xing, X. Di, and B. Wang: *J. Alloys Compd.*, 2014, vol. 593, pp. 110–16.
61. L. Ferrer, B. Pieraggi, J.F. Uginet: in *Superalloys 718, 612 and Various Derivatives*, E.A. Loria, ed., TMS, Warrendale, 1991.
62. M.G. Burke, M.K. Miller: *Superalloys 718, 612 and Various Derivatives,* E. A. Loria, ed., TMS, Warrendale, PA, 1991.
63. D.D. Krueger: in *Superalloy 718—Metallurgy and Application.* E.A. Loria, ed., TMS, 1989, pp. 279–96.
64. C.B. Shoemaker, A.H. Fox, and D.P. Shoemaker: *Acta Crystallogr.*, 1960, vol. 13, pp. 585–87.
65. J. Sheng, S. Huang, J.Z. Zhou, and Z.W. Wang: *Eng. Fract. Mech.*, 2017, vol. 169, pp. 99–108.
66. L.M. Suave, J. Cormier, D. Bertheau, P. Villechaise, A. Soula, Z. Hervier, and F. Hamon: *Mater. Sci. Eng. A*, 2016, vol. 650, pp. 161–70.
67. L.M. Suave, D. Bertheau, J. Cormier, P. Villechaise, A. Soula, Z. Hervier, J. Laigo: *Eurosuperalloys 2014, Giens, France, Matec Web of Conferences*, J.-Y. Guédouetal eds., 2014, p. 21001.